

---

# On the Decision Boundaries of Deep Neural Networks: A Tropical Geometry Perspective

---

Motasem Alfarra<sup>\*1</sup> Adel Bibi<sup>\*1</sup> Hasan Hammoud<sup>1</sup> Mohamed Gaafar<sup>2</sup> Bernard Ghanem<sup>1</sup>

## Abstract

This work tackles the problem of characterizing and understanding the decision boundaries of neural networks with piecewise linear non-linearity activations. We use tropical geometry, a new development in the area of algebraic geometry, to characterize the decision boundaries of a simple neural network of the form (Affine, ReLU, Affine). Our main finding is that the decision boundaries are a subset of a tropical hypersurface, which is intimately related to a polytope formed by the convex hull of two zonotopes. The generators of these zonotopes are functions of the neural network parameters. This geometric characterization provides new perspective to three tasks. Specifically, we propose a new tropical perspective to the lottery ticket hypothesis, where we see the effect of different initializations on the tropical geometric representation of a network's decision boundaries. Moreover, we use this characterization to propose a new set of tropical regularizers, which directly deal with the decision boundaries of a network. We investigate the use of these regularizers in neural network pruning (by removing network parameters that do not contribute to the tropical geometric representation of the decision boundaries) and in generating adversarial input attacks (by producing input perturbations that explicitly perturb the decision boundaries' geometry and ultimately change the network's prediction).

recognition (Hinton et al., 2012), natural language processing (Bahdanau et al., 2015; Devlin et al., 2018), quantum chemistry (Schütt et al., 2017), and healthcare (Ardila et al., 2019; Zhou et al., 2019) to name a few (LeCun et al., 2015). Nevertheless, a rigorous interpretation of their success remains elusive (Shalev-Shwartz & Ben-David, 2014). For instance, and in an attempt to uncover the expressive power of DNNs, the work of (Montufar et al., 2014) studied the complexity of functions computable by DNNs that have piecewise linear activations. They derived a lower bound on the maximum number of linear regions. Several other works have followed to improve such estimates under certain assumptions (Arora et al., 2018). In addition, and in attempt to understand some of the subtle behaviours DNNs exhibit, *e.g.* the sensitive reaction of DNNs to small input perturbations, several works directly investigated the decision boundaries induced by a DNN for classification. The work of (Seyed-Mohsen Moosavi-Dezfooli, 2019) showed that the smoothness of these decision boundaries and their curvature can play a vital role in network robustness. Moreover, the expressiveness of these decision boundaries at perturbed inputs was studied in (He et al., 2018a), where it was shown that these boundaries do not resemble the boundaries around benign inputs. The work of (Li et al., 2018) showed that under certain assumptions, the decision boundaries of the last fully connected layer of DNNs will converge to a linear SVM. Also, (Beise et al., 2018) showed that the decision regions of DNNs with width smaller than the input dimension are unbounded.

More recently, and due to the popularity of the piecewise linear ReLU as an activation function, there has been a surge in the number of works that study this class of DNNs in particular. As a result, this has incited significant interest in new mathematical tools that help analyze piecewise linear functions, such as tropical geometry. While tropical geometry has shown its potential in many applications such as dynamic programming (Joswig & Schröter, 2019), linear programming (Allamigeon et al., 2015), multi-objective discrete optimization (Joswig & Loho, 2019), enumerative geometry (Mikhalkin, 2004), and economics (Akian et al., 2009; Mai Tran & Yu, 2015), it has only been recently used to analyze DNNs. For instance, the work of Zhang et al. (2018) showed an equivalency between the family of DNNs

## 1. Introduction

Deep Neural Networks (DNNs) have demonstrated outstanding performance across a variety of research domains, including computer vision (Krizhevsky et al., 2012), speech

---

<sup>\*</sup>Equal contribution <sup>1</sup>King Abdullah University of Science and Technology (KAUST), Thuwal, Saudi Arabia <sup>2</sup>Fraunhofer Heinrich Hertz Institute, Berlin, Germany. Correspondence to: Motasem Alfarra <motasem.alfarra@kaust.edu.sa>, Adel Bibi <adel.bibi@kaust.edu.sa>.

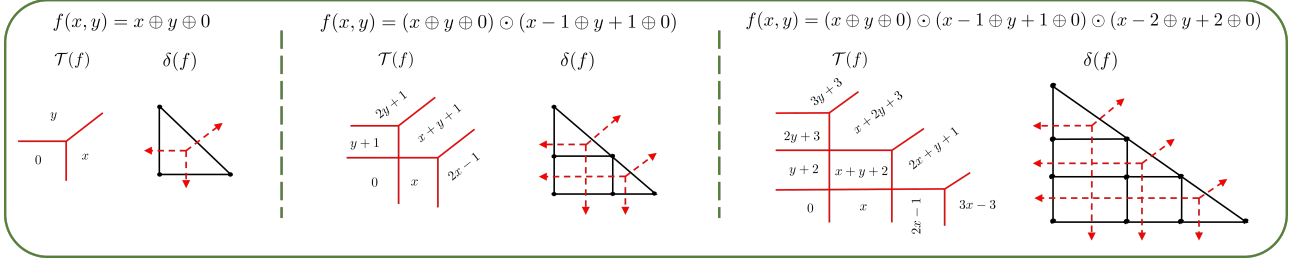


**Figure 1. Examples of tropical hypersurfaces and their corresponding dual subdivisions.** We show three tropical polynomials, where the solid red and black lines are the tropical hypersurfaces and dual subdivisions to the corresponding tropical polynomials, respectively. Note that the domain of  $f$  is divided by  $\mathcal{T}(f)$  into convex regions where  $f$  is linear in each region. Moreover, each region is in one-to-one correspondence with each edge vertex of the dual subdivision  $\delta(f)$ . Lastly, note that the tropical hypersurfaces are parallel to the normals of the edges of the dual subdivision polytope, indicated by dashed red lines.

with piecewise linear activations and integer weight matrices and the family of tropical rational maps, *i.e.* ratio between two multi-variate polynomials in tropical algebra. This study was mostly concerned about characterizing the complexity of a DNN by specifically counting the number of linear regions, into which the function represented by the DNN can divide the input space. This was done by counting the number of vertices of some polytope representation recovering the results of (Montufar et al., 2014) with a much simpler analysis.

**Contributions.** In this paper, we take the results of (Zhang et al., 2018) some steps further and present a novel perspective on the decision boundaries of DNNs using tropical geometry. To that end, our contributions are three-fold. (i) We derive a geometric representation (convex hull between two zonotopes) for a super set to the decision boundaries of a DNN in the form (Affine, ReLU, Affine). (ii) We demonstrate support for the lottery ticket hypothesis (Frankle & Carbin, 2019) using a geometric perspective. (iii) We leverage the geometric representation of the decision boundaries, referred to as the decision boundaries polytope, in two interesting applications: network pruning and adversarial attacks. For *tropical pruning*, we design a geometrically inspired optimization problem to prune the parameters of a given network such that the decision boundaries polytope of the pruned network does not deviate too much from the decision boundaries polytope of the original one. We conduct extensive experiments with AlexNet (Krizhevsky et al., 2012) and VGG16 (Simonyan & Zisserman, 2014) on SVHN (Netzer et al., 2011), CIFAR10, and CIFAR 100 (Krizhevsky & Hinton, 2009) datasets, in which 90% pruning rate can be achieved with a marginal drop in testing accuracy. For *tropical adversarial attacks*, we show that one can construct input adversaries that can change network predictions by perturbing the decision boundaries polytope.

## 2. Preliminaries to Tropical Geometry

For completeness, we first provide preliminaries to tropical geometry. For a detailed review, we refer readers to the work

of Itenberg et al. (2009); Maclagan & Sturmfels (2015).

**Definition 1. (Tropical Semiring<sup>1</sup>)** The tropical semiring  $\mathbb{T}$  is the triplet  $\{\mathbb{R} \cup \{-\infty\}, \oplus, \odot\}$ , where  $\oplus$  and  $\odot$  define tropical addition and tropical multiplication, respectively. They are denoted as:

$$x \oplus y = \max\{x, y\}, \quad x \odot y = x + y, \quad \forall x, y \in \mathbb{T}.$$

It can be readily shown that  $-\infty$  is the additive identity and 0 is the multiplicative identity.

Given the previous definition, a tropical power can be formulated as  $x^{\odot a} = x \odot x \cdots \odot x = a.x$ , for  $x \in \mathbb{T}$ ,  $a \in \mathbb{N}$ , where  $a.x$  is standard multiplication. Moreover, the tropical quotient can be defined as:  $x \oslash y = x - y$  where  $x - y$  is the standard subtraction. For ease of notation, we write  $x^{\odot a}$  as  $x^a$ . Now, we are in a position to define tropical polynomials, their solution sets, and tropical rationals.

**Definition 2. (Tropical Polynomials)** For  $\mathbf{x} \in \mathbb{T}^d$ ,  $c_i \in \mathbb{R}$  and  $\mathbf{a}_i \in \mathbb{N}^d$ , a  $d$ -variable tropical polynomial with  $n$  monomials  $f: \mathbb{T}^d \rightarrow \mathbb{T}^d$  can be expressed as:

$$f(\mathbf{x}) = (c_1 \odot \mathbf{x}^{\mathbf{a}_1}) \oplus (c_2 \odot \mathbf{x}^{\mathbf{a}_2}) \oplus \cdots \oplus (c_n \odot \mathbf{x}^{\mathbf{a}_n}), \\ \forall \mathbf{a}_i \neq \mathbf{a}_j \text{ when } i \neq j.$$

We use the more compact vector notation  $\mathbf{x}^{\mathbf{a}} = x_1^{a_1} \odot x_2^{a_2} \cdots \odot x_d^{a_d}$ . Moreover and for ease of notation, we will denote  $c_i \odot \mathbf{x}^{\mathbf{a}_i}$  as  $c_i \mathbf{x}^{\mathbf{a}_i}$  throughout the paper.

**Definition 3. (Tropical Rational Functions)** A tropical rational is a standard difference or a tropical quotient of two tropical polynomials:  $f(\mathbf{x}) - g(\mathbf{x}) = f(\mathbf{x}) \oslash g(\mathbf{x})$ .

Algebraic curves or hypersurfaces in algebraic geometry, which are the solution sets to polynomials, can be analogously extended to tropical polynomials too.

**Definition 4. (Tropical Hypersurfaces)** A tropical hypersurface of a tropical polynomial  $f(\mathbf{x}) = c_1 \mathbf{x}^{\mathbf{a}_1} \oplus \cdots \oplus c_n \mathbf{x}^{\mathbf{a}_n}$  is the set of points  $\mathbf{x}$  where  $f$  is attained by two or more

<sup>1</sup>A semiring is a ring that lacks an additive inverse.

monomials in  $f$ , i.e.

$$\mathcal{T}(f) := \{\mathbf{x} \in \mathbb{R}^d : c_i \mathbf{x}^{\mathbf{a}_i} = c_j \mathbf{x}^{\mathbf{a}_j} = f(\mathbf{x}), \\ \text{for some } \mathbf{a}_i \neq \mathbf{a}_j\}.$$

Tropical hypersurfaces divide the domain of  $f$  into convex regions, where  $f$  is linear in each region. Also, every tropical polynomial can be associated with a Newton polytope.

**Definition 5.** (*Newton Polytopes*) *The Newton polytope of a tropical polynomial  $f(\mathbf{x}) = c_1 \mathbf{x}^{\mathbf{a}_1} \oplus \dots \oplus c_n \mathbf{x}^{\mathbf{a}_n}$  is the convex hull of the exponents  $\mathbf{a}_i \in \mathbb{N}^d$  regarded as points in  $\mathbb{R}^d$ , i.e.*

$$\Delta(f) := \text{ConvHull}\{\mathbf{a}_i \in \mathbb{R}^d : i = 1, \dots, n \text{ and } c_i \neq -\infty\}.$$

A tropical polynomial determines a dual subdivision, which can thus be constructed by projecting the collection of upper faces (UF) in  $\mathcal{P}(f) := \text{ConvHull}\{(\mathbf{a}_i, c_i) \in \mathbb{R}^d \times \mathbb{R} : i = 1, \dots, n\}$  onto  $\mathbb{R}^d$ . That is to say, the dual subdivision determined by  $f$  is given as  $\delta(f) := \{\pi(p) \subset \mathbb{R}^d : p \in \text{UF}(\mathcal{P}(f))\}$ , where  $\pi : \mathbb{R}^d \times \mathbb{R} \rightarrow \mathbb{R}^d$  is the projection that drops the last coordinate. It has been shown by (Maclagan & Sturmfels, 2015) that the tropical hypersurface  $\mathcal{T}(f)$  is the  $(d-1)$ -skeleton of the polyhedral complex dual to  $\delta(f)$ . First, this implies that the vertex of each edge of the dual subdivision  $\delta(f)$  corresponds to one region in  $\mathbb{R}^d$ , where  $f$  is linear as determined by the tropical hypersurface  $\mathcal{T}(f)$ . This is exemplified in Figure 1 with three tropical polynomials, where the number of regions where  $f$  is linear for the three examples are 3, 6 and 10, respectively. Second, the tropical hypersurfaces are parallel to the normals of the edges of the dual subdivision polytope. The former in particular will be essential for the remaining part of the paper. Further details and standard results are summarized by (Brugallé & Shaw, 2014). Moreover, (Zhang et al., 2018) showed an equivalency between tropical rational maps and any neural network  $f : \mathbb{R}^n \rightarrow \mathbb{R}^k$  with piecewise linear activations and integer weights through the following theorem.

**Theorem 1.** (*Tropical Characterization of Neural Networks, (Zhang et al., 2018)*). *A feedforward neural network with integer weights and real biases with piecewise linear activation functions is a function  $f : \mathbb{R}^n \rightarrow \mathbb{R}^k$ , whose coordinates are tropical rational functions of the input, i.e.,*

$$f(\mathbf{x}) = H(\mathbf{x}) \odot Q(\mathbf{x}) = H(\mathbf{x}) - Q(\mathbf{x}),$$

where  $H$  and  $Q$  are tropical polynomials.

While this result is new in the context of tropical geometry, it is not surprising, since any piecewise linear function can be represented as a difference of two max functions over a set of hyperplanes (Melzer, 1986). Mathematically, if  $f$  is a piecewise linear function, it can be written as  $f(\mathbf{x}) = \max_{i \in [m]} \{\mathbf{a}_i^\top \mathbf{x}\} -$

$\max_{j \in [n]} \{\mathbf{b}_j^\top \mathbf{x}\}$ , where  $[m] = \{1, \dots, m\}$  and  $[n] = \{1, \dots, n\}$ . Thus, it is clear that each of the two maxima above is a tropical polynomial, recovering Theorem 1.

### 3. Decision Boundaries of Deep Neural Networks as Polytopes

In this section, we analyze the decision boundaries of a network in the form (Affine, ReLU, Affine) using tropical geometry. For ease, we use ReLUs as the non-linear activation, but any other piecewise linear function can also be used. The functional form of this network is:  $f(\mathbf{x}) = \mathbf{B} \max(\mathbf{A}\mathbf{x} + \mathbf{c}_1, \mathbf{0}) + \mathbf{c}_2$ , where  $\max(\cdot)$  is an element-wise operator. The outputs of the network  $f$  are the logit scores. Throughout this section, we assume<sup>2</sup> that  $\mathbf{A} \in \mathbb{Z}^{p \times n}$ ,  $\mathbf{B} \in \mathbb{Z}^{2 \times p}$ ,  $\mathbf{c}_1 \in \mathbb{R}^p$  and  $\mathbf{c}_2 \in \mathbb{R}^2$ . For ease of notation, we only consider networks with two outputs, i.e.  $\mathbf{B}^{2 \times p}$ , where the extension to a multi-class output follows naturally and is discussed in the **appendix**. Now, since  $f$  is a piecewise linear function, each output can be expressed as a tropical rational as per Theorem 1. If  $f_1$  and  $f_2$  refer to the first and second outputs respectively, we have  $f_1(\mathbf{x}) = H_1(\mathbf{x}) \odot Q_1(\mathbf{x})$  and  $f_2(\mathbf{x}) = H_2(\mathbf{x}) \odot Q_2(\mathbf{x})$ , where  $H_1, H_2, Q_1$  and  $Q_2$  are tropical polynomials. In what follows and for ease of presentation, we present our main results where the network  $f$  has no biases, i.e.  $\mathbf{c}_1 = \mathbf{0}$  and  $\mathbf{c}_2 = \mathbf{0}$ , and we leave the generalization to the **appendix**.

**Theorem 2.** *For a bias-free neural network in the form  $f(\mathbf{x}) : \mathbb{R}^n \rightarrow \mathbb{R}^2$ , where  $\mathbf{A} \in \mathbb{Z}^{p \times n}$  and  $\mathbf{B} \in \mathbb{Z}^{2 \times p}$ , let  $R(\mathbf{x}) = H_1(\mathbf{x}) \odot Q_2(\mathbf{x}) \oplus H_2(\mathbf{x}) \odot Q_1(\mathbf{x})$  be a tropical polynomial. Then:*

- Let  $\mathcal{B} = \{\mathbf{x} \in \mathbb{R}^n : f_1(\mathbf{x}) = f_2(\mathbf{x})\}$  define the decision boundaries of  $f$ , then  $\mathcal{B} \subseteq \mathcal{T}(R(\mathbf{x}))$ .
- $\delta(R(\mathbf{x})) = \text{ConvHull}(\mathcal{Z}_{\mathbf{G}_1}, \mathcal{Z}_{\mathbf{G}_2})$ .  $\mathcal{Z}_{\mathbf{G}_1}$  is a zonotope in  $\mathbb{R}^n$  with line segments  $\{(\mathbf{B}^+(1, j) + \mathbf{B}^-(2, j))[\mathbf{A}^+(j, :), \mathbf{A}^-(j, :)]\}_{j=1}^p$  and shift  $(\mathbf{B}^-(1, :) + \mathbf{B}^+(2, :))\mathbf{A}^-$ .  $\mathcal{Z}_{\mathbf{G}_2}$  is a zonotope in  $\mathbb{R}^n$  with line segments  $\{(\mathbf{B}^-(1, j) + \mathbf{B}^+(2, j))[\mathbf{A}^+(j, :), \mathbf{A}^-(j, :)]\}_{j=1}^p$  and shift  $(\mathbf{B}^+(1, :) + \mathbf{B}^-(2, :))\mathbf{A}^-$ . Note that  $\mathbf{A}^+ = \max(\mathbf{A}, 0)$  and  $\mathbf{A}^- = \max(-\mathbf{A}, 0)$ . The line segment  $(\mathbf{B}^+(1, j) + \mathbf{B}^-(2, j))[\mathbf{A}^+(j, :), \mathbf{A}^-(j, :)]$  has end points  $\mathbf{A}^+(j, :)$  and  $\mathbf{A}^-(j, :)$  in  $\mathbb{R}^n$  and scaled by  $(\mathbf{B}^+(1, j) + \mathbf{B}^-(2, j))$ .

The proof for Theorem 2 is left for the **appendix**.

**Digesting Theorem 2.** This theorem aims at characterizing the decision boundaries of a bias-free neural network of the form (Affine, ReLU, Affine) through the lens of tropical

<sup>2</sup>Without loss of generality, as one can very well approximate real weights as fractions by multiplying by least common multiple of the denominators as discussed in (Zhang et al., 2018).

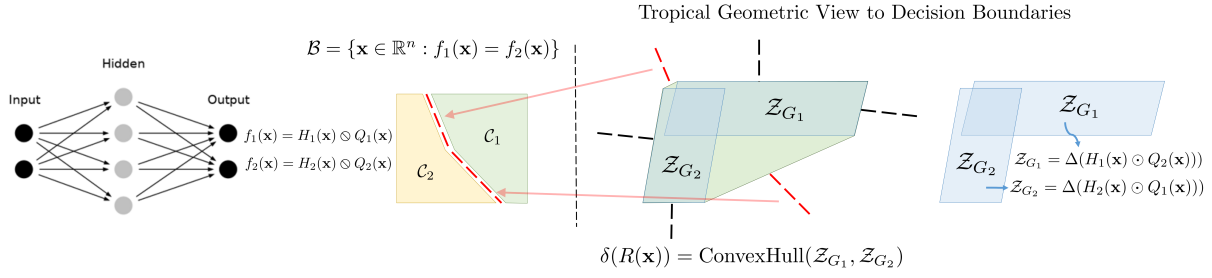


**Figure 2. Decision Boundaries as Geometric Structures.** The decision boundaries  $\mathcal{B}$  (in red) comprise two linear pieces separating classes  $\mathcal{C}_1$  and  $\mathcal{C}_2$ . As per Theorem 2, the dual subdivision of this single hidden neural network is the convex hull between the zonotopes  $\mathcal{Z}_{G_1}$  and  $\mathcal{Z}_{G_2}$ . The normals to the dual subdivision  $\delta(R(\mathbf{x}))$  are in one-to-one correspondence to the tropical hypersurface  $\mathcal{T}(R(\mathbf{x}))$ , which is a superset to the decision boundaries  $\mathcal{B}$ . Note that some of the normals to  $\delta(R(\mathbf{x}))$  (in red) are parallel to the decision boundaries.

geometry. In particular, the first result of Theorem 2 states that the tropical hypersurface  $\mathcal{T}(R(\mathbf{x}))$  of the tropical polynomial  $R(\mathbf{x})$  is a superset to the set of points forming the decision boundaries, *i.e.*  $\mathcal{B}$ . Just as discussed earlier and exemplified in Figure 1, tropical hypersurfaces are associated with a corresponding dual subdivision polytope  $\delta(R(\mathbf{x}))$ . Based on this, the second result of Theorem 2 states that this dual subdivision is precisely the convex hull of two zonotopes denoted as  $\mathcal{Z}_{G_1}$  and  $\mathcal{Z}_{G_2}$ , where each zonotope is only a function of the network parameters  $\mathbf{A}$  and  $\mathbf{B}$ .

Theorem 2 bridges the gap between the behaviour of the decision boundaries  $\mathcal{B}$ , through the superset  $\mathcal{T}(R(\mathbf{x}))$ , and the polytope  $\delta(R(\mathbf{x}))$ , which is the convex hull of two zonotopes. It is worthwhile to mention that (Zhang et al., 2018) discussed a special case of the first part of Theorem 2 for a neural network with a single output and a score function  $s(\mathbf{x})$  to classify the output. To the best of our knowledge, this work is the first to propose a tropical geometric formulation of a superset containing the decision boundaries of a multi-class classification neural network. In particular, the first result of Theorem 2 states that one can perhaps study the decision boundaries,  $\mathcal{B}$ , directly by studying their superset  $\mathcal{T}(R(\mathbf{x}))$ . While studying  $\mathcal{T}(R(\mathbf{x}))$  can be equally difficult, the second result of Theorem 2 comes in handy. First, note that, since the network is bias-free,  $\pi$  becomes an identity mapping with  $\delta(R(\mathbf{x})) = \Delta(R(\mathbf{x}))$ , and thus the dual subdivision  $\delta(R(\mathbf{x}))$ , which is the Newton polytope  $\Delta(R(\mathbf{x}))$  in this case, becomes a well-structured geometric object that can be exploited to preserve decision boundaries as per the second part of Theorem 2. Now, based on the results of (Maclagan & Sturmfels, 2015) (Proposition 3.1.6) and as discussed in Figure 1, the normals to the edges of the polytope  $\delta(R(\mathbf{x}))$  (convex hull of two zonotopes) are in one-to-one correspondence with the tropical hypersurface  $\mathcal{T}(R(\mathbf{x}))$ . Therefore, one can study the decision boundaries, or at least their superset  $\mathcal{T}(R(\mathbf{x}))$ , by studying the orientation of the dual subdivision  $\delta(R(\mathbf{x}))$ . Before any further discussion, we recap the definition of zonotopes.

**Definition 6.** Let  $\mathbf{u}^1, \dots, \mathbf{u}^p \in \mathbb{R}^n$ . The zonotope formed by  $\mathbf{u}^1, \dots, \mathbf{u}^p$  is defined as  $\mathcal{Z}(\mathbf{u}^1, \dots, \mathbf{u}^p) := \{\sum_{i=1}^p x_i \mathbf{u}^i : 0 \leq x_i \leq 1\}$ . Equivalently,  $\mathcal{Z}$  can be ex-

pressed with respect to the generator matrix  $\mathbf{U} \in \mathbb{R}^{p \times n}$ , where  $\mathbf{U}(i, :) = \mathbf{u}^i{}^\top$  as  $\mathcal{Z}_{\mathbf{U}} := \{\mathbf{U}^\top \mathbf{x} : \forall \mathbf{x} \in [0, 1]^p\}$ .

Another common definition for a zonotope is the Minkowski sum of a set of line segments that start from the origin in  $\mathbb{R}^n$  (refer to **appendix**). It is well known that the number of vertices of a zonotope is polynomial in the number of line segments *i.e.*  $|\text{vert}(\mathcal{Z}_{\mathbf{U}})| \leq 2 \sum_{i=0}^{n-1} \binom{p-1}{i} = \mathcal{O}(p^{n-1})$  (Gritzmann & Sturmfels, 1993).

While Theorem 2 presents a strong relation between a polytope (convex hull of two zonotopes) and the decision boundaries, it remains unclear how such a polytope can be efficiently constructed. Although the number of vertices of a zonotope is polynomial in the number of its generating line segments, fast algorithms for enumerating these vertices are still restricted to zonotopes with line segments starting at the origin (Stinson et al., 2016). Since the line segments generating the zonotopes in Theorem 2 have arbitrary end points, we present the next result that transforms these line segments into a generator matrix of line segments starting from the origin as in Definition 6. This result is essential for an efficient computation of the zonotopes in Theorem 2.

**Proposition 1.** The zonotope formed by  $p$  line segments in  $\mathbb{R}^n$  with two arbitrary end points as follows  $\{[\mathbf{u}_1^i, \mathbf{u}_2^i]\}_{i=1}^p$  is equivalent to the zonotope formed by the line segments  $\{[\mathbf{u}_1^i - \mathbf{u}_2^i, \mathbf{0}]\}_{i=1}^p$  with a shift of  $\sum_{i=1}^p \mathbf{u}_2^i$ .

The proof is left for the **appendix**. As per Proposition 1, the generator matrices of zonotopes  $\mathcal{Z}_{G_1}, \mathcal{Z}_{G_2}$  in Theorem 2 can be defined as  $\mathbf{G}_1 = \text{Diag}[(\mathbf{B}^+(1, :) + (\mathbf{B}^-(2, :)))]\mathbf{A}$  and  $\mathbf{G}_2 = \text{Diag}[(\mathbf{B}^+(2, :) + (\mathbf{B}^-(1, :)))]\mathbf{A}$ , both with shift  $(\mathbf{B}^-(1, :) + \mathbf{B}^+(2, :) + \mathbf{B}^+(1, :) + \mathbf{B}^-(2, :))\mathbf{A}^-$ , where  $\text{Diag}(\mathbf{v})$  rearranges the elements of  $\mathbf{v}$  in a diagonal matrix.

In what follows, we show several applications for Theorem 2. We begin by leveraging the geometric structure to help in reaffirming the behaviour of the lottery ticket hypothesis.



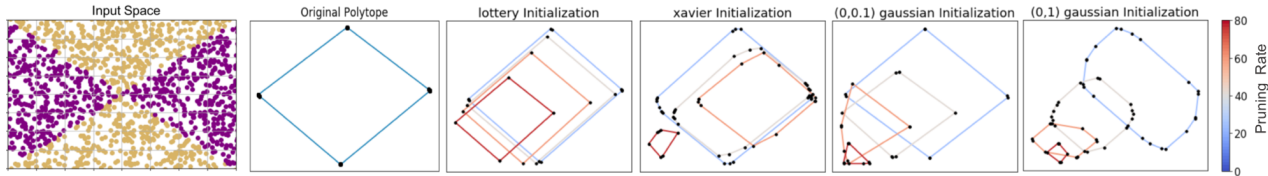


Figure 3. Effect of Different Initializations on the Decision Boundaries Polytope. From left to right: training dataset, decision boundaries polytope of original network (before pruning), followed by the decision boundaries polytope for networks pruned at different pruning percentages across different initializations. Note that in the original polytope there are many more vertices than just 4 but they are very close to each other forming many small edges that are not visible in the figure.

#### 4. Tropical Perspective to the Lottery Ticket Hypothesis

The lottery ticket hypothesis was recently proposed by (Frankle & Carbin, 2019), in which the authors surmise the existence of sparse trainable sub-networks of dense, randomly-initialized, feed-forward networks that when trained in isolation perform as well as the original network in a similar number of iterations.

To find such sub-networks, (Frankle & Carbin, 2019) propose the following simple algorithm: perform standard network pruning, initialize the pruned network with the same initialization that was used in the original training setting, and train with the same number of epochs. They hypothesize that this should result in a smaller network with a similar accuracy to the larger dense network. In other words, a subnetwork can have similar decision boundaries to the original network. While in this section we do not provide a theoretical reason for why this proposed pruning algorithm performs favorably, we utilize the geometric structure that arises from Theorem 2 to reaffirm such behaviour. In particular, we show that the orientation of the dual subdivision  $\delta(R(\mathbf{x}))$  (referred to as decision boundaries polytope from now on wards), where the normals to its edges are parallel to  $\mathcal{T}(R(\mathbf{x}))$  that is a superset to the decision boundaries, is preserved after pruning with the proposed initialization algorithm of (Frankle & Carbin, 2019). On the other hand, pruning routines with a different initialization at each pruning iteration will result in a severe variation in the orientation of the decision boundaries polytope. This leads to a large change in the orientation of the decision boundaries, which tends to hinder accuracy.

To this end, we train a neural network with 2 inputs ( $n = 2$ ), 2 outputs, and a single hidden layer with 40 nodes ( $p = 40$ ). We then prune the network by removing the smallest  $x\%$  of the weights. The pruned network is then trained using different initializations: (i) the same initialization as the original network (Frankle & Carbin, 2019), (ii) Xavier (Glorot & Bengio, 2010), (iii) standard Gaussian and (iv) zero mean Gaussian with variance of 0.1. Figure 3 shows the decision boundaries polytope, *i.e.*  $\delta(R(\mathbf{x}))$ , as we perform more pruning (increasing the  $x\%$ ) with different initializations. First, we show the decision boundaries by sampling and

classifying points in a grid with the trained network (first subfigure). We then plot the decision boundaries polytope  $\delta(R(\mathbf{x}))$  as per the second part of Theorem 2 denoted as original polytope (second subfigure). While there are many overlapping vertices in the original polytope, the normals to some of the edges (the major visible edges) are parallel in direction to the decision boundaries shown in the first subfigure of Figure 3. We later show the decision boundaries polytope for the same network with varying levels of pruning. It is to be observed that the orientation of the polytopes  $\delta(R(\mathbf{x}))$  deviate from the decision boundaries polytope of the original network without any pruning much more for all different initialization schemes as compared to the lottery ticket initialization. This gives an indication that lottery ticket initialization indeed preserves the decision boundaries, since it preserves the orientation of the decision boundaries polytope throughout the evolution of pruning. Several other examples are left for the **appendix**. Another approach to investigate the lottery ticket could be by observing the polytopes representing the functional form of the network directly, *i.e.*  $\delta(H_{\{1,2\}}(\mathbf{x}))$  and  $\delta(Q_{\{1,2\}}(\mathbf{x}))$ , in lieu of the decision boundaries polytopes. However, this does not provide conclusive answers to the lottery ticket, since there can exist multiple functional forms, and correspondingly multiple polytopes  $\delta(H_{\{1,2\}}(\mathbf{x}))$  and  $\delta(Q_{\{1,2\}}(\mathbf{x}))$ , for networks with the same decision boundaries. This is why we explicitly focus our analysis on  $\delta(R(\mathbf{x}))$ , which is directly related to the decision boundaries of the network. Further discussions and experiments are left for the **appendix**.

#### 5. Tropical Network Pruning

Network pruning has been identified as an effective approach for reducing the computational cost and memory usage during network inference. While it dates back to the work of (LeCun et al., 1990) and (Hassibi & Stork, 1993), network pruning has recently gained more attention. This is due to the fact that most neural networks over-parameterize commonly used datasets. In network pruning, the task is to find a smaller subset of the network parameters, such that the resulting smaller network has similar decision boundaries (and thus supposedly similar accuracy) to the original over-parameterized network. In this section, we show a new

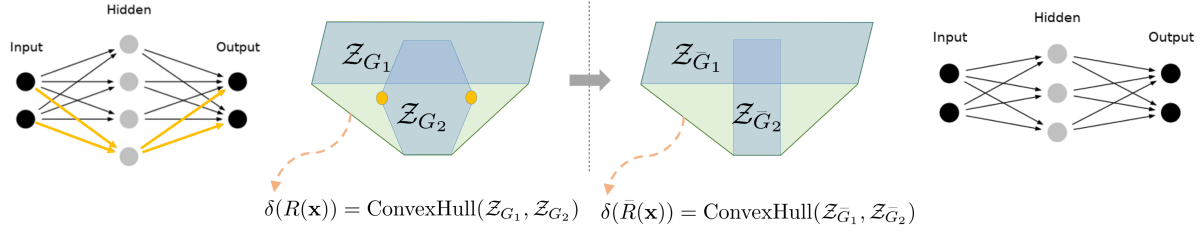


Figure 4. **Tropical Pruning Pipeline.** Pruning the 4<sup>th</sup> node, or equivalently removing the two yellow vertices of zonotope  $Z_{G_2}$  does not affect the decision boundaries polytope, which will lead to no change in accuracy.

geometric approach towards network pruning. In particular, as indicated by Theorem 2, preserving the polytope  $\delta(R(\mathbf{x}))$  preserves a superset to the decision boundaries  $\mathcal{T}(R(\mathbf{x}))$ , and thus supposedly the decision boundaries themselves.

**Motivational Insight.** For a single hidden layer neural network, the dual subdivision to the decision boundaries is the polytope that is the convex hull of two zonotopes, where each is formed by taking the Minkowski sum of line segments (Theorem 2). Figure 4 shows an example, where pruning a neuron in the neural network has no effect on the dual subdivision polytope and equivalently no effect on the accuracy. This is since the orientation of the decision boundaries polytope did not change, thus, preserving the tropical hypersurface  $\mathcal{T}(R(\mathbf{x}))$  and keeping the decision boundaries of both networks the same.

**Problem Formulation.** In light of the motivational insight, a natural question arises: *Given an over-parameterized binary output neural network  $f(\mathbf{x}) = \mathbf{B} \max(\mathbf{A}\mathbf{x}, \mathbf{0})$ , can one construct a new neural network, parameterized by some sparser weight matrices  $\tilde{\mathbf{A}}$  and  $\tilde{\mathbf{B}}$ , such that this smaller network has a dual subdivision  $\delta(\tilde{R}(\mathbf{x}))$  that preserves the decision boundaries of the original network?*

To address this question, we propose the following general optimization problem to compute  $\tilde{\mathbf{A}}$  and  $\tilde{\mathbf{B}}$ :

$$\begin{aligned} & \min_{\tilde{\mathbf{A}}, \tilde{\mathbf{B}}} d\left(\delta(\tilde{R}(\mathbf{x})), \delta(R(\mathbf{x}))\right) \\ & = \min_{\tilde{\mathbf{A}}, \tilde{\mathbf{B}}} d\left(\text{ConvHull}(Z_{\tilde{G}_1}, Z_{\tilde{G}_2}), \text{ConvHull}(Z_{G_1}, Z_{G_2})\right). \end{aligned} \quad (1)$$

The function  $d(\cdot)$  defines a distance between two geometric objects. Since the generators  $\tilde{G}_1$  and  $\tilde{G}_2$  are functions of  $\tilde{\mathbf{A}}$  and  $\tilde{\mathbf{B}}$  (as per Theorem 2), this optimization problem can be challenging to solve. However, for pruning purposes, one can observe from Theorem 2 that if the generators  $\tilde{G}_1$  and  $\tilde{G}_2$  had fewer number of line segments (rows), this corresponds to a fewer number of rows in the weight matrix  $\tilde{\mathbf{A}}$  (sparser weights). So, we observe that if  $\tilde{G}_1 \approx G_1$  and  $\tilde{G}_2 \approx G_2$ , then  $\delta(\tilde{R}(\mathbf{x})) \approx \delta(R(\mathbf{x}))$ , and thus the decision boundaries tend to be preserved as a consequence. Therefore, we propose the following optimization problem

as a surrogate to Problem (1):

$$\begin{aligned} & \min_{\tilde{\mathbf{A}}, \tilde{\mathbf{B}}} \frac{1}{2} \left( \left\| \tilde{\mathbf{G}}_1 - \mathbf{G}_1 \right\|_F^2 + \left\| \tilde{\mathbf{G}}_2 - \mathbf{G}_2 \right\|_F^2 \right) \\ & \quad + \lambda_1 \left\| \tilde{\mathbf{G}}_1 \right\|_{2,1} + \lambda_2 \left\| \tilde{\mathbf{G}}_2 \right\|_{2,1}. \end{aligned} \quad (2)$$

The matrix mixed norm for  $\mathbf{C} \in \mathbb{R}^{n \times k}$  is defined as  $\|\mathbf{C}\|_{2,1} = \sum_{i=1}^n \|\mathbf{C}(i, :)\|_2$ , which encourages the matrix  $\mathbf{C}$  to be row sparse, *i.e.* complete rows of  $\mathbf{C}$  are zero. Note that  $\tilde{\mathbf{G}}_1 = \text{Diag}[\text{ReLU}(\tilde{\mathbf{B}}(1, :)) + \text{ReLU}(-\tilde{\mathbf{B}}(2, :))] \tilde{\mathbf{A}}$  and  $\tilde{\mathbf{G}}_2 = \text{Diag}[\text{ReLU}(\tilde{\mathbf{B}}(2, :)) + \text{ReLU}(-\tilde{\mathbf{B}}(1, :))] \tilde{\mathbf{A}}$ . We solve Problem (2) through alternating optimization over the variables  $\tilde{\mathbf{A}}$  and  $\tilde{\mathbf{B}}$ , where each sub-problem can be solved in closed form. Details of the optimization and the extension to the multi-class case are left for the **appendix**.

**Extension to Deeper Networks.** For deeper networks, one can still apply the aforementioned optimization for consecutive blocks. In particular, we prune each consecutive block of the form (Affine, ReLU, Affine) starting from the input and ending at the output of the network.

**Experiments on Tropical Pruning.** Here, we evaluate the performance of the proposed pruning approach as compared to several classical approaches on several architectures and datasets. In particular, we compare our tropical pruning approach against Class Blind (CB), Class Uniform (CU) and Class Distribution (CD) (Han et al., 2015; See et al., 2016). In Class Blind, all the parameters across all nodes of a layer are sorted by magnitude where  $x\%$  with smallest magnitude are pruned. In contrast, Class Uniform prunes the parameters with smallest  $x\%$  magnitudes per node in a layer. Lastly, Class Distribution performs pruning of all parameters for each node in the layer, just as in Class Uniform, but the parameters are pruned based on the standard deviation  $\sigma_c$  of the magnitude of the parameters per node. Since fully connected layers in deep neural networks tend to have much higher memory complexity than convolutional layers, we restrict our focus to pruning fully connected layers. We train AlexNet and VGG16 on SVHN, CIFAR10, and CIFAR100 datasets. We observe that we can prune more than 90% of the classifier parameters for both networks without affecting the accuracy. Moreover, we demonstrate experimentally that our approach can outperform all other methods even

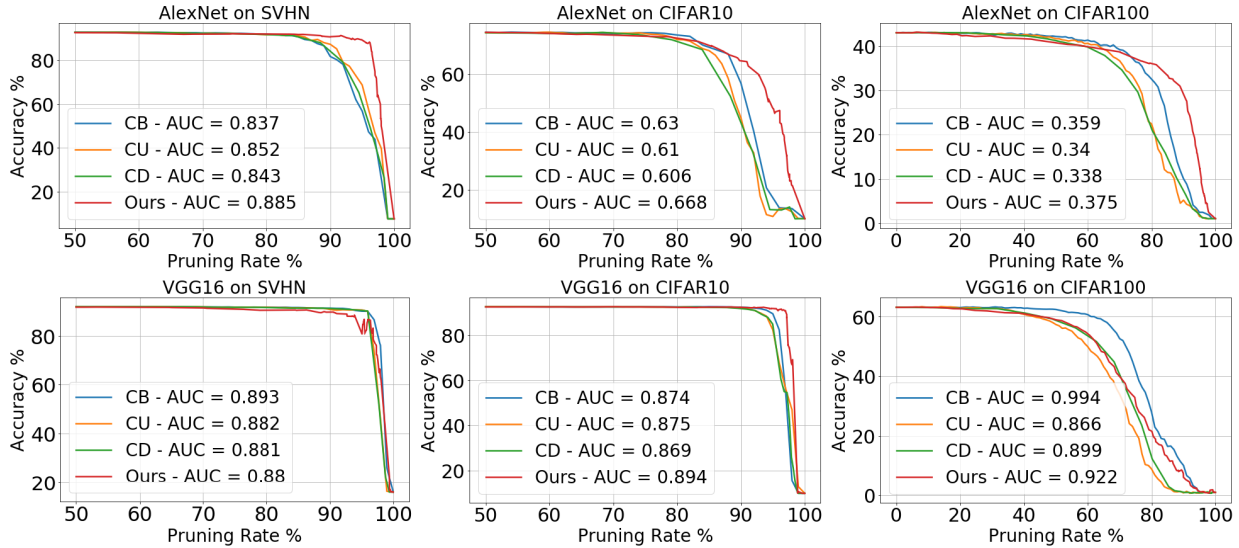


Figure 5. **Results of Tropical Pruning.** Pruning-accuracy plots for AlexNet (top) and VGG16 (bottom) trained on SVHN, CIFAR10, and CIFAR100, pruned with our tropical method and three other pruning methods.

when all parameters or when only the biases are fine tuned after pruning (these experiments in addition to many others are left for the **appendix**).

*Setup.* We adapt the architectures of AlexNet and VGG16, since they were originally trained on ImageNet (Deng et al., 2009), to account for the discrepancy in the input resolution. The fully connected layers of AlexNet and VGG16 have sizes of (256,512,10) and (512,512,10), respectively on SVHN and CIFAR100 with the last layer replaced to 100 for CIFAR100. All networks were trained to baseline test accuracy of (92%,74%,43%) for AlexNet on SVHN, CIFAR10 and CIFAR100, respectively and (92%,92%,70%) for VGG16. To evaluate the performance of pruning and following previous work (Han et al., 2015), we report the area under the curve (AUC) of the pruning-accuracy plot. The higher the AUC is, the better the trade-off is between pruning rate and accuracy. For efficiency purposes, we run the optimization in Problem (2) for a single alternating iteration to identify the rows in  $\hat{\mathbf{A}}$  and elements of  $\hat{\mathbf{B}}$  that will be pruned, since an exact pruning solution might not be necessary. The algorithm and the parameter setup to solving Problem (2) is left for the **appendix**.

*Results.* Figure 4 shows the comparison between our tropical approach and the three popular pruning schemes on both AlexNet and VGG16 over the different datasets. Our proposed approach can indeed prune out as much as 90% of the parameters of the classifier without sacrificing much of the accuracy. For AlexNet, we achieve much better performance in pruning as compared to other methods. In particular, we are better in AUC by 3%, 3%, and 2% over other pruning methods on SVHN, CIFAR10 and CIFAR100, respectively. This indicates that the decision boundaries can indeed be preserved by preserving the dual subdivi-

sion polytope. For VGG16, we perform similarly well on both SVHN and CIFAR10 and slightly worse on CIFAR100. While the performance achieved here is comparable to the other pruning schemes, if not better, we emphasize that our contribution does not lie in outperforming state-of-the-art pruning methods, but in giving a new geometry-based perspective to network pruning. We conduct more experiments where only the biases of the network or only the classifier are fine tuned after pruning. Retraining biases can be sufficient as they do not contribute to the orientation of the decision boundaries polytope (and effectively the decision boundaries) but only a translation. Discussion on biases and more results are left for **appendix**.

## 6. Tropical Adversarial Attacks

DNNs are notorious for being susceptible to adversarial attacks. In fact, adding small imperceptible noise, referred to as adversarial attacks, to the input of these networks can hinder their performance. Several works investigated the decision boundaries of neural networks in the presence of adversarial attacks. For instance, (Khoury & Hadfield-Menell, 2018) analyzed the high dimensional geometry of adversarial examples by means of manifold reconstruction. Also, (He et al., 2018b) crafted adversarial attacks by estimating the distance to the decision boundaries using random search directions. In this work, we provide a tropical geometric view to this task, where we show how Theorem 2 can be leveraged to construct a tropical geometry-based targeted adversarial attack.

**Dual View to Adversarial Attacks.** For a classifier  $f : \mathbb{R}^n \rightarrow \mathbb{R}^k$  and input  $\mathbf{x}_0$  classified as  $c$ , a standard formulation for targeted adversarial attacks flips the prediction

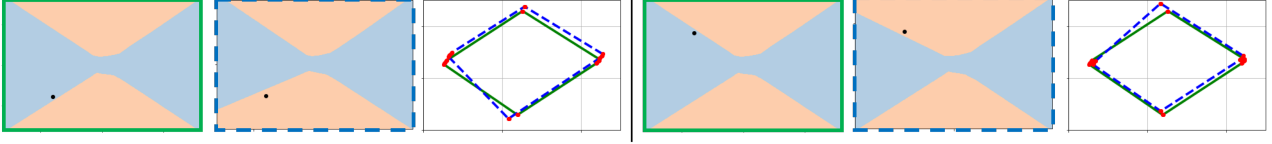


Figure 6. **Dual View of Tropical Adversarial Attacks.** We show the effects of tropical adversarial attacks on a synthetic binary dataset at two different input points (in black). From left to right: the decision regions of the original and perturbed models, and decision boundaries polytopes (green for original and blue for perturbed).

to a particular class  $t$  and is usually defined as

$$\min_{\eta} \mathcal{D}(\eta) \quad \text{s.t.} \quad \arg \max_i f_i(\mathbf{x}_0 + \eta) = t \neq c \quad (3)$$

This objective aims to compute the lowest energy input noise  $\eta$  (measured by  $\mathcal{D}$ ) such that the new sample  $(\mathbf{x}_0 + \eta)$  crosses the decision boundaries of  $f$  to a new classification region. Here, we present a dual view to adversarial attacks. Instead of designing a sample noise  $\eta$  such that  $(\mathbf{x}_0 + \eta)$  belongs to a new decision region, one can instead fix  $\mathbf{x}_0$  and perturb the network parameters to move the decision boundaries in a way that  $\mathbf{x}_0$  appears in a new classification region. In particular, let  $\mathbf{A}_1$  be the first linear layer of  $f$ , such that  $f(\mathbf{x}_0) = g(\mathbf{A}_1 \mathbf{x}_0)$ . One can now perturb  $\mathbf{A}_1$  to alter the decision boundaries and relate this parameter perturbation to the input perturbation as follows:

$$\begin{aligned} g((\mathbf{A}_1 + \xi_{\mathbf{A}_1})\mathbf{x}_0) &= g(\mathbf{A}_1 \mathbf{x}_0 + \xi_{\mathbf{A}_1} \mathbf{x}_0) \\ &= g(\mathbf{A}_1 \mathbf{x}_0 + \mathbf{A}_1 \eta) = f(\mathbf{x}_0 + \eta). \end{aligned} \quad (4)$$

From this dual view, we observe that traditional adversarial attacks are intimately related to perturbing the parameters of the first linear layer through the linear system:  $\mathbf{A}_1 \eta = \xi_{\mathbf{A}_1} \mathbf{x}_0$ . *The two views and formulations are identical* under such condition. With this analysis, Theorem 2 provides explicit means to geometrically construct adversarial attacks by perturbing the decision boundaries. In particular, since the normals to the dual subdivision polytope  $\delta(R(\mathbf{x}))$  of a given neural network represent the tropical hypersurface  $\mathcal{T}(R(\mathbf{x}))$ , which is a superset to the decision boundaries set  $\mathcal{B}$ ,  $\xi_{\mathbf{A}_1}$  can be designed to result in a minimal perturbation to the dual subdivision that is sufficient to change the network prediction of  $\mathbf{x}_0$  to the targeted class  $t$ . Based on this observation, we formulate the problem as follows:

$$\begin{aligned} \min_{\eta, \xi_{\mathbf{A}_1}} \quad & \mathcal{D}_1(\eta) + \mathcal{D}_2(\xi_{\mathbf{A}_1}) \\ \text{s.t.} \quad & -\text{loss}(g(\mathbf{A}_1(\mathbf{x}_0 + \eta)), t) \leq -1; \\ & -\text{loss}(g(\mathbf{A}_1 + \xi_{\mathbf{A}_1})\mathbf{x}_0, t) \leq -1; \\ & (\mathbf{x}_0 + \eta) \in [0, 1]^n, \quad \|\eta\|_{\infty} \leq \epsilon_1; \\ & \|\xi_{\mathbf{A}_1}\|_{\infty, \infty} \leq \epsilon_2, \quad \mathbf{A}_1 \eta = \xi_{\mathbf{A}_1} \mathbf{x}_0. \end{aligned} \quad (5)$$

The loss is the standard cross-entropy loss. The first row of constraints ensures that the network prediction is the desired target class  $t$  when the input  $\mathbf{x}_0$  is perturbed by

$\eta$ , and equivalently by perturbing the first linear layer  $\mathbf{A}_1$  by  $\xi_{\mathbf{A}_1}$ . This is identical to  $f_1$  as proposed by (Carlini & Wagner, 2016). Moreover, the third and fourth constraints guarantee that the perturbed input is feasible and that the perturbation is bounded, respectively. The fifth constraint is to limit the maximum perturbation on the first linear layer, while the last constraint enforces the dual equivalence between input perturbation and parameter perturbation. The function  $\mathcal{D}_2$  captures the perturbation of the dual subdivision polytope upon perturbing the first linear layer by  $\xi_{\mathbf{A}_1}$ . For a single hidden layer neural network parameterized as  $(\mathbf{A}_1 + \xi_{\mathbf{A}_1}) \in \mathbb{R}^{p \times n}$  and  $\mathbf{B} \in \mathbb{R}^{2 \times p}$  for the first and second layers respectively,  $\mathcal{D}_2$  can capture the perturbations in each of the two zonotopes discussed in Theorem 2 and we define it as:

$$\begin{aligned} \mathcal{D}_2(\xi_{\mathbf{A}_1}) &= \frac{1}{2} \sum_{j=1}^2 \left\| \text{Diag}(\mathbf{B}^+(j, :)) \xi_{\mathbf{A}_1} \right\|_F^2 \\ &\quad + \left\| \text{Diag}(\mathbf{B}^-(j, :)) \xi_{\mathbf{A}_1} \right\|_F^2. \end{aligned} \quad (6)$$

The derivation, discussion, and extension of (6) to multi-class neural networks is left for the **appendix**. We solve Problem (5) with a penalty method on the linear equality constraints, where each penalty step is solved with ADMM (Boyd et al., 2011) in a similar fashion to the work of (Xu et al., 2018). The details of the algorithm are left for the **appendix**.

**Motivational Insight to the Dual View.** Here, we train a single hidden layer neural network, where the size of the input is 2 with 50 hidden nodes and 2 outputs on a simple dataset as shown in Figure 6. We then solve Problem 5 for a given  $\mathbf{x}_0$  shown in black. We show the decision boundaries for the network with and without the perturbation at the first linear layer  $\xi_{\mathbf{A}_1}$ . Figure 6 shows that perturbing an edge of the dual subdivision polytope, by perturbing the first linear layer, indeed corresponds to perturbing the decision boundaries and results in the misclassification of  $\mathbf{x}_0$ . Interestingly and as expected, perturbing different decision boundaries corresponds to perturbing different edges of the dual subdivision. Furthermore, we conduct extensive experiments on MNIST images, which show that successful adversarial attacks  $\eta$  can be designed by solving Problem (5). Due to space constraints, we leave these results for the **appendix**.



## 7. Conclusion

We leverage tropical geometry to characterize the decision boundaries of neural networks in the form (Affine, ReLU, Affine) and relate it to geometric objects such as zonotopes. We then provide a tropical perspective to support the lottery ticket hypothesis, prune networks, and design adversarial attacks. A natural extension is a compact derivation for the characterization of the decision boundaries of convolutional neural networks and graphical convolutional networks.

**Acknowledgments.** This work was supported by the King Abdullah University of Science and Technology (KAUST) Office of Sponsored Research.

## References

- Akian, M., Gaubert, S., and Guterman, A. Tropical polyhedra are equivalent to mean payoff games. *International Journal of Algebra and Computation*, 2009.
- Allamigeon, X., Benchimol, P., Gaubert, S., and Joswig, M. Tropicalizing the simplex algorithm. *SIAM J. Discrete Math.* 29:2, 2015.
- Ardila, D., P. Kiraly, A., Bharadwaj, S., Choi, B., J. Reichert, J., Peng, L., Tse, D., Etemadi, M., Ye, W., Corrado, G., P. Naidich, D., and Shetty, S. End-to-end lung cancer screening with three-dimensional deep learning on low-dose chest computed tomography. *Nature Medicine*, 2019.
- Arora, R., Basu, A., Mianjy, P., and Mukherjee, A. Understanding deep neural networks with rectified linear units. In *International Conference on Learning Representations*, 2018.
- Bahdanau, D., Cho, K., and Bengio, Y. Neural machine translation by jointly learning to align and translate. In *International Conference on Learning Representations*, 2015.
- Beise, H.-P., Da Cruz, S. D., and Schröder, U. On decision regions of narrow deep neural networks. *arXiv preprint arXiv:1807.01194*, 2018.
- Berrada, L., Zisserman, A., and Kumar, M. P. Trusting svm for piecewise linear cnns. *arXiv preprint arXiv:1611.02185*, 2016.
- Boyd, S., Parikh, N., Chu, E., Peleato, B., Eckstein, J., et al. Distributed optimization and statistical learning via the alternating direction method of multipliers. *Foundations and Trends® in Machine learning*, 2011.
- Brugallé, E. and Shaw, K. A bit of tropical geometry. *The American Mathematical Monthly*, 2014.
- Carlini, N. and Wagner, D. A. Towards evaluating the robustness of neural networks. *CoRR*, 2016.
- Deng, J., Dong, W., Socher, R., Li, L.-J., Li, K., and Fei-Fei, L. Imagenet: A large-scale hierarchical image database. In *Computer Vision and Patter Recognition Conference (CVPR)*, 2009.
- Devlin, J., Chang, M.-W., Lee, K., and Toutanova, K. Bert: Pre-training of deep bidirectional transformers for language understanding. *arXiv preprint arXiv:1810.04805*, 2018.
- Frankle, J. and Carbin, M. The lottery ticket hypothesis: Finding sparse, trainable neural networks. In *ICLR. Open-Review.net*, 2019.
- Glorot, X. and Bengio, Y. Understanding the difficulty of training deep feedforward neural networks. In *Proceedings of 13th International Conference on Artificial Intelligence and Statistics*, 2010.
- Gritzmann, P. and Sturmfels, B. Minkowski addition of polytopes: computational complexity and applications to gröbner bases. *SIAM Journal on Discrete Mathematics*, 1993.
- Han, S., Pool, J., Tran, J., and Dally, W. J. Learning both weights and connections for efficient neural networks. *CoRR*, 2015.
- Hassibi, B. and Stork, D. G. Second order derivatives for network pruning: Optimal brain surgeon. In *Advances in neural information processing systems*, 1993.
- He, W., Li, B., and Song, D. Decision boundary analysis of adversarial examples. In *International Conference on Learning Representations (ICLR)*, 2018a.
- He, W., Li, B., and Song, D. Decision boundary analysis of adversarial examples. In *International Conference on Learning Representations*, 2018b.
- Hinton, G., Deng, L., Yu, D., Dahl, G. E., Mohamed, A., Jaitly, N., Senior, A., Vanhoucke, V., Nguyen, P., Sainath, T. N., and Kingsbury, B. Deep neural networks for acoustic modeling in speech recognition: The shared views of four research groups. *IEEE Signal Processing Magazine*, 2012.
- Itenberg, I., Mikhalkin, G., and Shustin, E. I. *Tropical algebraic geometry*. Springer Science & Business Media, 2009.
- Joswig, M. and Loho, G. Monomial tropical cones for multicriteria optimization. *AIP Conference Proceedings*, 2019.

- Joswig, M. and Schröter, B. The tropical geometry of shortest paths. *arXiv preprint arXiv:1904.01082*, 2019.
- Khoury, M. and Hadfield-Menell, D. On the geometry of adversarial examples. *arXiv preprint arXiv:1811.00525*, 2018.
- Krizhevsky, A. and Hinton, G. Learning multiple layers of features from tiny images. Technical report, Citeseer, 2009.
- Krizhevsky, A., Sutskever, I., and Hinton, G. E. ImageNet classification with deep convolutional neural networks. In *Advances in Neural Information Processing Systems (NeurIPS)*, 2012.
- LeCun, Y., Denker, J. S., and Solla, S. A. Optimal brain damage. In *Advances in neural information processing systems*, 1990.
- LeCun, Y., Bengio, Y., and Hinton, G. Deep learning. *Nature*, 2015.
- Li, Y., Richtarik, P., Ding, L., and Gao, X. On the decision boundary of deep neural networks. *arXiv preprint arXiv:1808.05385*, 2018.
- Liu, Q., Shen, X., and Gu, Y. Linearized admm for nonconvex nonsmooth optimization with convergence analysis. *IEEE Access*, 2019.
- Maclagan, D. and Sturmfels, B. *Introduction to Tropical Geometry*. Graduate Studies in Mathematics. American Mathematical Society, 2015.
- Mai Tran, N. and Yu, J. Product-mix auctions and tropical geometry. *Mathematics of Operations Research*, 2015.
- Melzer, D. On the expressibility of piecewise-linear continuous functions as the difference of two piecewise-linear convex functions. In *Quasidifferential Calculus*. Springer, 1986.
- Mikhalkin, G. Enumerative tropical algebraic geometry in  $\mathbb{R}^2$ . *Journal of the American Mathematical Society*, 2004.
- Montufar, G., Pascanu, R., Cho, K., and Bengio, Y. On the number of linear regions of deep neural networks. *Advances in Neural Information Processing Systems (NeurIPS)*, 2014.
- Netzer, Y., Wang, T., Coates, A., Bissacco, A., Wu, B., and Ng, A. Y. Reading digits in natural images with unsupervised feature learning. *Advances in Neural Information Processing Systems (NeurIPS)*, 2011.
- Schütt, K., Arbabzadah, F., Chmiela, S., Müller, K.-R., and Tkatchenko, A. Quantum-chemical insights from deep tensor neural networks. *Nature Communications*, 2017.
- See, A., Luong, M., and Manning, C. D. Compression of neural machine translation models via pruning. *CoRR*, 2016.
- Seyed-Mohsen Moosavi-Dezfooli, Alhussein Fawzi, J. U. P. F. Robustness via curvature regularization, and vice versa. *CVPR*, 2019.
- Shalev-Shwartz, S. and Ben-David, S. *Understanding machine learning: From theory to algorithms*. Cambridge university press, 2014.
- Simonyan, K. and Zisserman, A. Very deep convolutional networks for large-scale image recognition. *arXiv preprint arXiv:1409.1556*, 2014.
- Stinson, K., Gleich, D. F., and Constantine, P. G. A randomized algorithm for enumerating zonotope vertices. *arXiv preprint arXiv:1602.06620*, 2016.
- Xu, K., Liu, S., Zhao, P., Chen, P., Zhang, H., Erdogmus, D., Wang, Y., and Lin, X. Structured adversarial attack: Towards general implementation and better interpretability. *arXiv preprint arXiv:1808.01664*, 2018.
- Zhang, L., Naitzat, G., and Lim, L.-H. Tropical geometry of deep neural networks. In *International Conference on Machine Learning, ICML 2018*, 2018.
- Zhou, J., Y. Park, C., L. Theesfeld, C., Wong, A., Yuan, Y., Scheckel, C., Fak, J., Funk, J., Yao, K., Tajima, Y., Packer, A., Darnell, R., and G. Troyanskaya, O. Whole-genome deep-learning analysis identifies contribution of noncoding mutations to autism risk. *Nature Genetics*, 2019.

## A. Preliminaries and Definitions.

**Fact 1.**  $P \tilde{+} Q = \{p + q, \forall p \in P \text{ and } q \in Q\}$  is the Minkowski sum between two sets  $P$  and  $Q$ .

**Fact 2.** Let  $f$  be a tropical polynomial and let  $a \in \mathbb{N}$ . Then

$$\mathcal{P}(f^a) = a\mathcal{P}(f).$$

Let both  $f$  and  $g$  be tropical polynomials, Then

**Fact 3.**

$$\mathcal{P}(f \odot g) = \mathcal{P}(f) \tilde{+} \mathcal{P}(g). \tag{7}$$

**Fact 4.**

$$\mathcal{P}(f \oplus g) = \text{ConvexHull}\left(\mathcal{V}(\mathcal{P}(f)) \cup \mathcal{V}(\mathcal{P}(g))\right). \tag{8}$$

Note that  $\mathcal{V}(\mathcal{P}(f))$  is the set of vertices of the polytope  $\mathcal{P}(f)$ .

## B. Proof Of Theorem 2

**Theorem 2.** For a bias-free neural network in the form of  $f(\mathbf{x}) : \mathbb{R}^n \rightarrow \mathbb{R}^2$  where  $\mathbf{A} \in \mathbb{Z}^{p \times n}$  and  $\mathbf{B} \in \mathbb{Z}^{2 \times p}$ , let  $R(\mathbf{x}) = H_1(\mathbf{x}) \odot Q_2(\mathbf{x}) \oplus H_2(\mathbf{x}) \odot Q_1(\mathbf{x})$  be a tropical polynomial. Then:

- Let  $\mathcal{B} = \{\mathbf{x} \in \mathbb{R}^n : f_1(\mathbf{x}) = f_2(\mathbf{x})\}$  define the decision boundaries of  $f$ , then  $\mathcal{B} \subseteq \mathcal{T}(R(\mathbf{x}))$ .
- $\delta(R(\mathbf{x})) = \text{ConvHull}(\mathcal{Z}_{\mathbf{G}_1}, \mathcal{Z}_{\mathbf{G}_2})$ .  $\mathcal{Z}_{\mathbf{G}_1}$  is a zonotope in  $\mathbb{R}^n$  with line segments  $\{(\mathbf{B}^+(1, j) + \mathbf{B}^-(2, j))[\mathbf{A}^+(j, :), \mathbf{A}^-(j, :)]\}_{j=1}^p$  and shift  $(\mathbf{B}^-(1, :) + \mathbf{B}^+(2, :))\mathbf{A}^-$ .  $\mathcal{Z}_{\mathbf{G}_2}$  is a zonotope in  $\mathbb{R}^n$  with line segments  $\{(\mathbf{B}^-(1, j) + \mathbf{B}^+(2, j))[\mathbf{A}^+(j, :), \mathbf{A}^-(j, :)]\}_{j=1}^p$  and shift  $(\mathbf{B}^+(1, :) + \mathbf{B}^-(2, :))\mathbf{A}^-$ . Note that  $\mathbf{A}^+ = \max(\mathbf{A}, 0)$  and  $\mathbf{A}^- = \max(-\mathbf{A}, 0)$ . The line segment  $(\mathbf{B}^+(1, j) + \mathbf{B}^-(2, j))[\mathbf{A}^+(j, :), \mathbf{A}^-(j, :)]$  has end points  $\mathbf{A}^+(j, :)$  and  $\mathbf{A}^-(j, :)$  in  $\mathbb{R}^n$  and scaled by  $(\mathbf{B}^+(1, j) + \mathbf{B}^-(2, j))$ .

Note that  $\mathbf{A}^+ = \max(\mathbf{A}, 0)$  and  $\mathbf{A}^- = \max(-\mathbf{A}, 0)$  where the  $\max(\cdot)$  is element-wise. The line segment  $(\mathbf{B}(1, j)^+ + \mathbf{B}(2, j)^-)[\mathbf{A}(j, :)^+, \mathbf{A}(j, :)^-]$  is one that has the end points  $\mathbf{A}(j, :)^+$  and  $\mathbf{A}(j, :)^-$  in  $\mathbb{R}^n$  and scaled by the constant  $\mathbf{B}(1, j)^+ + \mathbf{B}(2, j)^-$ .

*Proof.* For the first part, recall from Theorem 1 that both  $f_1$  and  $f_2$  are tropical rationals and hence,

$$f_1(\mathbf{x}) = H_1(\mathbf{x}) - Q_1(\mathbf{x}) \quad f_2(\mathbf{x}) = H_2(\mathbf{x}) - Q_2(\mathbf{x})$$

Thus

$$\begin{aligned} \mathcal{B} &= \{x \in \mathbb{R}^n : f_1(\mathbf{x}) = f_2(\mathbf{x})\} = \{x \in \mathbb{R}^n : H_1(\mathbf{x}) - Q_1(\mathbf{x}) = H_2(\mathbf{x}) - Q_2(\mathbf{x})\} \\ &= \{x \in \mathbb{R}^n : H_1(\mathbf{x}) + Q_2(\mathbf{x}) = H_2(\mathbf{x}) + Q_1(\mathbf{x})\} \\ &= \{x \in \mathbb{R}^n : H_1(\mathbf{x}) \odot Q_2(\mathbf{x}) = H_2(\mathbf{x}) \odot Q_1(\mathbf{x})\} \end{aligned}$$

Recall that the tropical hypersurface is defined as the set of  $\mathbf{x}$  where the maximum is attained by two or more monomials. Therefore, the tropical hypersurface of  $R(\mathbf{x})$  is the set of  $\mathbf{x}$  where the maximum is attained by two or more monomials in  $(H_1(\mathbf{x}) \odot Q_2(\mathbf{x}))$ , or attained by two or more monomials in  $(H_2(\mathbf{x}) \odot Q_1(\mathbf{x}))$ , or attained by monomials in both of them in the same time, which is the decision boundaries. Hence, we can rewrite that as

$$\mathcal{T}(R(\mathbf{x})) = \mathcal{T}(H_1(\mathbf{x}) \odot Q_2(\mathbf{x})) \cup \mathcal{T}(H_2(\mathbf{x}) \odot Q_1(\mathbf{x})) \cup \mathcal{B}.$$

Therefore  $\mathcal{B} \subseteq \mathcal{T}(R(\mathbf{x}))$ . For the second part of the Theorem, we first use the decomposition proposed by (Zhang et al., 2018; Berrada et al., 2016) to show that for a network  $f(\mathbf{x}) = \mathbf{B} \max(\mathbf{A}\mathbf{x}, \mathbf{0})$ , it can be decomposed as tropical rational as follows

$$\begin{aligned} f(\mathbf{x}) &= (\mathbf{B}^+ - \mathbf{B}^-) \left( \max(\mathbf{A}^+\mathbf{x}, \mathbf{A}^-\mathbf{x}) - \mathbf{A}^-\mathbf{x} \right) \\ &= \left[ \mathbf{B}^+ \max(\mathbf{A}^+\mathbf{x}, \mathbf{A}^-\mathbf{x}) + \mathbf{B}^- \mathbf{A}^-\mathbf{x} \right] \\ &\quad - \left[ \mathbf{B}^- \max(\mathbf{A}^+\mathbf{x}, \mathbf{A}^-\mathbf{x}) + \mathbf{B}^+ \mathbf{A}^-\mathbf{x} \right]. \end{aligned}$$

Therefore, we have that

$$\begin{aligned} H_1(\mathbf{x}) + Q_2(\mathbf{x}) &= \left( \mathbf{B}^+(1, :) + \mathbf{B}^-(2, :) \right) \max(\mathbf{A}^+\mathbf{x}, \mathbf{A}^-\mathbf{x}) \\ &\quad + \left( \mathbf{B}^-(1, :) + \mathbf{B}^+(2, :) \right) \mathbf{A}^-\mathbf{x} \end{aligned}$$

$$\begin{aligned} H_2(\mathbf{x}) + Q_1(\mathbf{x}) &= \left( \mathbf{B}^-(1, :) + \mathbf{B}^+(2, :) \right) \max(\mathbf{A}^+\mathbf{x}, \mathbf{A}^-\mathbf{x}) \\ &\quad + \left( \mathbf{B}^+(1, :) + \mathbf{B}^-(2, :) \right) \mathbf{A}^-\mathbf{x}. \end{aligned}$$



Therefore, note that:

$$\begin{aligned} \delta(R(\mathbf{x})) &= \delta\left(\left(H_1(\mathbf{x}) \odot Q_2(\mathbf{x})\right) \oplus \left(H_2(\mathbf{x}) \odot Q_1(\mathbf{x})\right)\right) \\ &\stackrel{(8)}{=} \text{ConvexHull}\left(\delta\left(H_1(\mathbf{x}) \odot Q_2(\mathbf{x})\right), \delta\left(H_2(\mathbf{x}) \odot Q_1(\mathbf{x})\right)\right) \\ &\stackrel{(7)}{=} \text{ConvexHull}\left(\delta\left(H_1(\mathbf{x})\right) \tilde{+} \delta\left(Q_2(\mathbf{x})\right), \delta\left(H_2(\mathbf{x})\right) \tilde{+} \delta\left(Q_1(\mathbf{x})\right)\right). \end{aligned}$$

Now observe that  $H_1(\mathbf{x}) = \sum_{j=1}^p \left(\mathbf{B}^+(1, j) + \mathbf{B}^-(2, j)\right) \max\left(\mathbf{A}^+(j, :), \mathbf{A}^-(j, :)\mathbf{x}\right)$  tropically is given as follows  $H_1(\mathbf{x}) = \odot_{j=1}^p \left[\mathbf{x}^{\mathbf{A}^+(j, :)} \oplus \mathbf{x}^{\mathbf{A}^-(j, :)}\right]^{\mathbf{B}^+(1, j) \odot \mathbf{B}^-(2, j)}$ , thus we have that :

$$\begin{aligned} \delta(H_1(\mathbf{x})) &= \left(\mathbf{B}^+(1, 1) + \mathbf{B}^-(2, 1)\right) \delta\left(\mathbf{x}^{\mathbf{A}^+(1, :)} \oplus \mathbf{x}^{\mathbf{A}^-(1, :)}\right) \tilde{+} \dots \\ &\quad \tilde{+} \left(\mathbf{B}^+(1, p) + \mathbf{B}^-(2, p)\right) \left(\delta\left(\mathbf{x}^{\mathbf{A}^+(p, :)} \oplus \mathbf{x}^{\mathbf{A}^-(p, :)}\right)\right) \\ &= \left(\mathbf{B}^+(1, 1) + \mathbf{B}^-(2, 1)\right) \text{ConvexHull}\left(\mathbf{A}^+(1, :), \mathbf{A}^-(1, :)\right) \tilde{+} \dots \\ &\quad \tilde{+} \left(\mathbf{B}^+(1, p) + \mathbf{B}^-(2, p)\right) \text{ConvexHull}\left(\mathbf{A}^+(p, :), \mathbf{A}^-(p, :)\right). \end{aligned}$$

The operator  $\tilde{+}$  indicates a Minkowski sum between sets. Note that  $\text{ConvexHull}\left(\mathbf{A}^+(i, :), \mathbf{A}^-(i, :)\right)$  is the convexhull between two points which is a line segment in  $\mathbb{Z}^n$  with end points that are  $\{\mathbf{A}^+(i, :), \mathbf{A}^-(i, :)\}$  scaled with  $\mathbf{B}^+(1, i) + \mathbf{B}^-(2, i)$ . Observe that  $\delta(H_1(\mathbf{x}))$  is a Minkowski sum of line segments which is a zonotope. Moreover, note that  $Q_2(\mathbf{x}) = (\mathbf{B}^-(1, :) + \mathbf{B}^+(2, :))\mathbf{A}^-\mathbf{x}$  tropically is given as follows  $Q_2(\mathbf{x}) = \odot_{j=1}^p \mathbf{x}^{\mathbf{A}^-(j, :)} (\mathbf{B}^+(1, j) \odot \mathbf{B}^-(2, j))$ . One can see that  $\delta(Q_2(\mathbf{x}))$  is the Minkowski sum of the points  $\{(\mathbf{B}^-(1, j) - \mathbf{B}^+(2, j))\mathbf{A}^-(j, :)\} \forall j$  in  $\mathbb{R}^n$  (which is a standard sum) resulting in a point. Lastly,  $\delta(H_1(\mathbf{x})) \tilde{+} \delta(Q_2(\mathbf{x}))$  is a Minkowski sum between a zonotope and a single point which corresponds to a shifted zonotope. A similar symmetric argument can be applied for the second part  $\delta(H_2(\mathbf{x})) \tilde{+} \delta(Q_1(\mathbf{x}))$ .  $\square$

It is also worthy to mention that the extension to network with multi class output is trivial. In that case all of the analysis can be exactly applied studying the decision boundary between any two classes  $(i, j)$  where  $\mathcal{B} = \{x \in \mathbb{R}^n : f_i(\mathbf{x}) = f_j(\mathbf{x})\}$  and the rest of the proof will be exactly the same.

## C. Handling Biases

In this section, we show that the results of Theorem 2 are the unaltered in the presence of biases ( $\mathbf{c}_1$  and  $\mathbf{c}_2$ ). To do so, we will derive the dual subdivision of the output of the first Affine layer, the ReLU and the last Affine layer consecutively.

As for the output of the first affine layer, note that for an input  $\mathbf{x}$  the output of the first affine layer  $\mathbf{z}_1 = \mathbf{A}\mathbf{x} + \mathbf{c}_1$  can be presented tropically per coordinate as:

$$\mathbf{z}_{1_i} = \mathbf{A}^+(i, :)\mathbf{x} + \mathbf{c}_1(i) - \mathbf{A}^-(i, :)\mathbf{x} = (\mathbf{c}_1(i) \odot \mathbf{x}^{\mathbf{A}^+(i, :)} \odot \mathbf{x}^{\mathbf{A}^-(i, :)} = H_{1_i} \odot Q_{1_i}. \quad (9)$$

To construct the dual subdivision for each tropical polynomial  $H_{1_i}$  and  $Q_{1_i}$ , one needs first to construct the tropical newton polytope in  $\mathbb{R}^{n+1}$  as defined in Definition 5. Since both of  $H_{1_i}$  and  $Q_{1_i}$  are tropical polynomials with a single monomials thus  $\Delta(H_{1_i})$  and  $\Delta(Q_{1_i})$  are the points  $(\mathbf{A}^+(i, :), \mathbf{c}_1(i))$  and  $(\mathbf{A}^-(i, :), 0)$  in  $\mathbb{R}^{n+1}$ , respectively. To construct the dual subdivision of each tropical polynomial, one needs to project the newton polytope to  $\mathbb{R}^n$  through the operator  $\pi$  which will again result in an identical dual subdivision if biases were not introduced.

As for the output of the ReLU layer, note that for an input  $\mathbf{x}$ , it can be presented tropically per coordinate as follows

$$\mathbf{z}_{2_i} = \max(\mathbf{z}_1, \mathbf{0}) = \max(\mathbf{A}^+(i, :)\mathbf{x} + \mathbf{c}_1(i), \mathbf{A}^-(i, :)\mathbf{x}) - \mathbf{A}^-(i, :)\mathbf{x} = (H_{1_i} \oplus Q_{1_i}) - Q_{1_i} = H_{2_i} \otimes Q_{2_i}.$$

Following Fact 4, the newton polytope of  $H_{2_i}$  is a line segment, *i.e.*  $\Delta(H_{2_i})$ , with end points  $[(\mathbf{A}^+(i, :), \mathbf{c}_1(i)), (\mathbf{A}^-(i, :), \mathbf{0})]$ . Constructing the dual subdivision by projecting both  $\Delta(H_{2_i})$  and  $\Delta(Q_{1_i})$  to  $\mathbb{R}^n$  recovers an identical dual subdivision for a bias free-network. Similarly for  $\Delta(Q_{2_i})$  which is a point in  $\mathbb{R}^{n+1}$  with coordinate  $[\mathbf{A}^-(i, :), 0]$ . Applying the projection  $\pi$  recovers to construct the dual subdivision recovers the point  $[\mathbf{A}^-(i, :)]$  in  $\mathbb{R}^n$ .

Lastly, the output of the second affine layer per coordinate can be expressed as:

$$\begin{aligned} \mathbf{z}_{3_i} &= \mathbf{B}(i, :)\mathbf{z}_2 + \mathbf{c}_2(i) = (\mathbf{B}^+(i, :) - \mathbf{B}^-(i, :))(H_{2_i} - Q_{2_i}) + \mathbf{c}_2(i) \\ &= (\mathbf{B}^+(i, :)H_{2_i} + \mathbf{B}^-(i, :)Q_{2_i} + \mathbf{c}_2(i)) - (\mathbf{B}^-(i, :)H_{2_i} + \mathbf{B}^+(i, :)Q_{2_i}) \\ &= (\mathbf{B}^+(i, :)H_{2_i} + \mathbf{B}^-(i, :)Q_{2_i} + \mathbf{c}_2(i)) - (\mathbf{B}^-(i, :)H_{2_i} + \mathbf{B}^+(i, :)Q_{2_i}) \\ &= H_{3_i} \otimes Q_{3_i}. \end{aligned}$$

Following Facts 2 and 3, we have that  $\Delta(H_{3_i}) = \tilde{\vdash}_j \left( \mathbf{B}(i, j)\Delta(H_{2_j}) \right) \tilde{\vdash} \Delta \left( \odot_j \mathbf{B}^-(i, j)\Delta(Q_{2_j}) \Big|_{\mathbb{R}^n}, \mathbf{c}_2(i) \right)$  where  $\Delta(Q_{2_j}) \Big|_{\mathbb{R}^n}$  is the newton polytope of  $Q_{2_j}$  just as before but in  $\mathbb{R}^n$ . Note that the first term, *i.e.*  $\tilde{\vdash}_j \left( \mathbf{B}(i, j)\Delta(H_{2_j}) \right)$  is a Minkowski sum of scaled line segments  $\Delta(H_{2_j})$  that are in  $\mathbb{R}^{n+1}$  resulting in a zonotope in  $\mathbb{R}^{n+1}$ . The second term is the polytope that results from the Minkowski sum, as per Fact 2, of the scaled polytopes  $\Delta(Q_{2_j}) \Big|_{\mathbb{R}^n}$  where each polytope is a point in  $\mathbb{R}^n$  with the last coordinate be  $\mathbf{c}_2(i)$ . Therefore, the polytope  $\Delta(H_{3_i})$  is a Minkowski sum between a zonotope and a point resulting in a shifted zonotope in  $\mathbb{R}^{n+1}$ . Constructing the dual subdivision  $\delta(H_{3_i})$  results in the same polytope projected in  $\mathbb{R}^n$ . This is an identical dual subdivision to a bias free network. Therefore, the shape of the geometric representation of the decision boundaries with non-zero biases will not be altered the projection  $\pi$ , and hence the presence of the biases will not alter the results of Theorem 2.

## D. Proof of Proposition 1

**Proposition 1.** *The zonotope formed by  $p$  line segments in  $\mathbb{R}^n$  with two arbitrary end points as follows  $\{[\mathbf{u}_1^i, \mathbf{u}_2^i]\}_{i=1}^p$  is equivalent to the zonotope formed by the line segments  $\{[\mathbf{u}_1^i - \mathbf{u}_2^i, \mathbf{0}]\}_{i=1}^p$  with a shift of  $\sum_{i=1}^p \mathbf{u}_2^i$ .*

*Proof.* Let  $\mathbf{U}_j$  be a matrix with  $\mathbf{U}_j(:, i) = \mathbf{u}_j^i, i = 1, \dots, p$ ,  $\mathbf{w}$  be a column-vector with  $\mathbf{w}(i) = w_i, i = 1, \dots, p$  and  $\mathbf{1}_p$  is a column-vector of ones of length  $p$ . Then, the zonotope  $\mathcal{Z}$  formed by the Minkowski sum of line segments with arbitrary end points can be defined as:

$$\begin{aligned} \mathcal{Z} &= \left\{ \sum_{i=1}^p w_i \mathbf{u}_1^i + (1 - w_i) \mathbf{u}_2^i; w_i \in [0, 1], \forall i \right\} \\ &= \left\{ \mathbf{U}_1 \mathbf{w} - \mathbf{U}_2 \mathbf{w} + \mathbf{U}_2 \mathbf{1}_p, \mathbf{w} \in [0, 1]^p \right\} \\ &= \left\{ (\mathbf{U}_1 - \mathbf{U}_2) \mathbf{w} + \mathbf{U}_2 \mathbf{1}_p, \mathbf{w} \in [0, 1]^p \right\} \\ &= \left\{ (\mathbf{U}_1 - \mathbf{U}_2) \mathbf{w}, \mathbf{w} \in [0, 1]^p \right\} \tilde{\vdash} \left\{ \mathbf{U}_2 \mathbf{1}_p \right\}. \end{aligned}$$

Since the Minkowski sum of between a polytope and a point is a translation; thereafter, the proposition follows directly from Definition 6.  $\square$

### D.1. Optimization of Objective (2) of the Binary Classifier

$$\min_{\tilde{\mathbf{A}}, \tilde{\mathbf{B}}} \frac{1}{2} \left\| \tilde{\mathbf{G}}_1 - \mathbf{G}_1 \right\|_F^2 + \left\| \frac{1}{2} \tilde{\mathbf{G}}_2 - \mathbf{G}_2 \right\|_F^2 + \lambda_1 \left\| \tilde{\mathbf{G}}_1 \right\|_{2,1} + \lambda_2 \left\| \tilde{\mathbf{G}}_2 \right\|_{2,1}. \quad (10)$$

Note that  $\tilde{\mathbf{G}}_1 = \text{Diag} \left[ \text{ReLU}(\tilde{\mathbf{B}}(1, :)) + \text{ReLU}(-\tilde{\mathbf{B}}(2, :)) \right] \tilde{\mathbf{A}}$ ,  $\tilde{\mathbf{G}}_2 = \text{Diag} \left[ \text{ReLU}(\tilde{\mathbf{B}}(2, :)) + \text{ReLU}(-\tilde{\mathbf{B}}(1, :)) \right] \tilde{\mathbf{A}}$ . Note that  $\mathbf{G}_1 = \text{Diag} \left[ \text{ReLU}(\mathbf{B}(1, :)) + \text{ReLU}(-\mathbf{B}(2, :)) \right] \mathbf{A}$  and  $\mathbf{G}_2 = \text{Diag} \left[ \text{ReLU}(\mathbf{B}(2, :)) + \text{ReLU}(-\mathbf{B}(1, :)) \right] \mathbf{A}$ . For ease of notation, we refer to  $\text{ReLU}(\tilde{\mathbf{B}}(i, :))$  and  $\text{ReLU}(-\tilde{\mathbf{B}}(i, :))$  as  $\tilde{\mathbf{B}}^+(i, :)$  and  $\tilde{\mathbf{B}}^-(i, :)$ , respectively. We solve the problem with co-ordinate descent an alternate over variables.

**Update  $\tilde{\mathbf{A}}$ .**

$$\tilde{\mathbf{A}} \leftarrow \arg \min_{\tilde{\mathbf{A}}} \frac{1}{2} \left\| \text{Diag}(\mathbf{c}_1) \tilde{\mathbf{A}} - \mathbf{G}_1 \right\|_F^2 + \frac{1}{2} \left\| \text{Diag}(\mathbf{c}_2) \tilde{\mathbf{A}} - \mathbf{G}_2 \right\|_F^2 + \lambda_1 \left\| \text{Diag}(\mathbf{c}_1) \tilde{\mathbf{A}} \right\|_{2,1} + \lambda_2 \left\| \text{Diag}(\mathbf{c}_2) \tilde{\mathbf{A}} \right\|_{2,1},$$

where  $\mathbf{c}_1 = \text{ReLU}(\mathbf{B}(1, :)) + \text{ReLU}(-\mathbf{B}(2, :))$  and  $\mathbf{c}_2 = \text{ReLU}(\mathbf{B}(2, :)) + \text{ReLU}(-\mathbf{B}(1, :))$ . Note that the problem is separable per-row of  $\tilde{\mathbf{A}}$ . Therefore, the problem reduces to updating rows of  $\tilde{\mathbf{A}}$  independently and the problem exhibits a closed form solution.

$$\begin{aligned} \tilde{\mathbf{A}}(i, :) &= \arg \min_{\tilde{\mathbf{A}}(i, :)} \frac{1}{2} \left\| \mathbf{c}_1^i \tilde{\mathbf{A}}(i, :) - \mathbf{G}_1(i, :) \right\|_2^2 + \frac{1}{2} \left\| \mathbf{c}_2^i \tilde{\mathbf{A}}(i, :) - \mathbf{G}_2(i, :) \right\|_2^2 + (\lambda_1 \sqrt{\mathbf{c}_1^i} + \lambda_2 \sqrt{\mathbf{c}_2^i}) \left\| \tilde{\mathbf{A}}(i, :) \right\|_2 \\ &= \arg \min_{\tilde{\mathbf{A}}(i, :)} \frac{1}{2} \left\| \tilde{\mathbf{A}}(i, :) - \frac{\mathbf{c}_1^i \mathbf{G}_1(i, :) + \mathbf{c}_2^i \mathbf{G}_2(i, :)}{\frac{1}{2}(\mathbf{c}_1^i + \mathbf{c}_2^i)} \right\|_2^2 + \frac{1}{2} \frac{\lambda_1 \sqrt{\mathbf{c}_1^i} + \lambda_2 \sqrt{\mathbf{c}_2^i}}{\frac{1}{2}(\mathbf{c}_1^i + \mathbf{c}_2^i)} \left\| \tilde{\mathbf{A}}(i, :) \right\|_2 \\ &= \left( 1 - \frac{1}{2} \frac{\lambda_1 \sqrt{\mathbf{c}_1^i} + \lambda_2 \sqrt{\mathbf{c}_2^i}}{\frac{1}{2}(\mathbf{c}_1^i + \mathbf{c}_2^i)} \frac{1}{\left\| \frac{\mathbf{c}_1^i \mathbf{G}_1(i, :) + \mathbf{c}_2^i \mathbf{G}_2(i, :)}{\frac{1}{2}(\mathbf{c}_1^i + \mathbf{c}_2^i)} \right\|_2} \right) \left( \frac{\mathbf{c}_1^i \mathbf{G}_1(i, :) + \mathbf{c}_2^i \mathbf{G}_2(i, :)}{\frac{1}{2}(\mathbf{c}_1^i + \mathbf{c}_2^i)} \right). \end{aligned}$$

**Update  $\tilde{\mathbf{B}}^+(1, :)$ .**

$$\tilde{\mathbf{B}}^+(1, :) = \arg \min_{\tilde{\mathbf{B}}^+(1, :)} \frac{1}{2} \left\| \text{Diag} \left( \tilde{\mathbf{B}}^+(1, :) \right) \tilde{\mathbf{A}} - \mathbf{C}_1 \right\|_F^2 + \lambda_1 \left\| \text{Diag} \left( \tilde{\mathbf{B}}^+(1, :) \right) \tilde{\mathbf{A}} + \mathbf{C}_2 \right\|_{2,1}, \quad \text{s.t. } \tilde{\mathbf{B}}^+(1, :) \geq \mathbf{0}.$$

Note that  $\mathbf{C}_1 = \mathbf{G}_1 - \text{Diag} \left( \tilde{\mathbf{B}}^-(2, :) \right) \tilde{\mathbf{A}}$  and where  $\text{Diag} \left( \tilde{\mathbf{B}}^-(2, :) \right) \tilde{\mathbf{A}}$ . Note the problem is separable in the coordinates of  $\tilde{\mathbf{B}}^+(1, :)$  and a projected gradient descent can be used to solve the problem in such a way as:

$$\tilde{\mathbf{B}}^+(1, j) = \arg \min_{\tilde{\mathbf{B}}^+(1, j)} \frac{1}{2} \left\| \tilde{\mathbf{B}}^+(1, j) \tilde{\mathbf{A}}(j, :) - \mathbf{C}_1(j, :) \right\|_2^2 + \lambda_1 \left\| \tilde{\mathbf{B}}^+(1, j) \tilde{\mathbf{A}}(j, :) + \mathbf{C}_2(j, :) \right\|_2, \quad \text{s.t. } \tilde{\mathbf{B}}^+(1, j) \geq 0.$$

A similar symmetric argument can be used to update the variables  $\tilde{\mathbf{B}}^+(2, :)$ ,  $\tilde{\mathbf{B}}^+(1, :)$  and  $\tilde{\mathbf{B}}^-(2, :)$ .

### D.2. Adapting Optimization (2) for Multi-Class Classifier

Note that Theorem 2 describes a superset to the decision boundaries of a binary classifier through the dual subdivision  $R(\mathbf{x})$ , *i.e.*  $\delta(R(\mathbf{x}))$ . For a neural network  $f$  with  $k$  classes, a natural extension for it is to analyze the pair-wise decision boundaries of of all  $k$ -classes. Thus, let  $\mathcal{T}(R_{ij}(\mathbf{x}))$  be the superset to the decision boundaries separating classes  $i$  and  $j$ . Therefore, a natural extension to the geometric loss in Equation (1) is to preserve the polytopes among all pairwise follows:

$$\min_{\tilde{\mathbf{A}}, \tilde{\mathbf{B}}} \sum_{\forall [i, j] \in S} d \left( \text{ConvexHull} \left( \mathcal{Z}_{\tilde{\mathbf{G}}_{(i+, j-)}}, \mathcal{Z}_{\tilde{\mathbf{G}}_{(j+, i-)}} \right), \text{ConvexHull} \left( \mathcal{Z}_{\mathbf{G}_{(i+, j-)}}, \mathcal{Z}_{\mathbf{G}_{(j+, i-)}} \right) \right). \quad (11)$$

The set  $S$  is all possible pairwise combinations of the  $k$  classes such that  $S = \{[i, j], \forall i \neq j, i = 1, \dots, k, j = 1, \dots, k\}$ . The generator  $\mathcal{Z}(\tilde{\mathbf{G}}_{(i,j)})$  is the zonotope with the generator matrix  $\tilde{\mathbf{G}}_{(i,j)} = \text{Diag} \left[ \text{ReLU}(\tilde{\mathbf{B}}(i, :)) + \text{ReLU}(-\tilde{\mathbf{B}}(j, :)) \right] \tilde{\mathbf{A}}$ . However, such an approach is generally computationally expensive, particularly, when  $k$  is very large. To this end, we make the following observation that  $\tilde{\mathbf{G}}_{(i^+, j^-)}$  can be equivalently written as a Minkowski sum between two sets zonotopes with the generators  $\mathbf{G}_{(i^+)} = \text{Diag} \left[ \text{ReLU}(\tilde{\mathbf{B}}(i, :)) \right] \tilde{\mathbf{A}}$  and  $\mathbf{G}_{(j^-)} = \text{Diag} \left[ \text{ReLU}(\tilde{\mathbf{B}}(j, :)) \right] \tilde{\mathbf{A}}$ . That is to say,  $\mathcal{Z}_{\tilde{\mathbf{G}}_{(i^+, j^-)}} = \mathcal{Z}_{\tilde{\mathbf{G}}_{i^+}} \tilde{+} \mathcal{Z}_{\tilde{\mathbf{G}}_{j^-}}$ . This follows from the associative property of Minkowski sums given as follows:

**Fact 5.** Let  $\{S_i\}_{i=1}^n$  be the set of  $n$  line segments. Then we have that

$$S = S_1 \tilde{+} \dots \tilde{+} S_n = P \tilde{+} V$$

where the sets  $P = \tilde{+}_{j \in C_1} S_j$  and  $V = \tilde{+}_{j \in C_2} S_j$  where  $C_1$  and  $C_2$  are any complementary partitions of the set  $\{S_i\}_{i=1}^n$ .

Hence,  $\tilde{\mathbf{G}}_{(i^+, j^-)}$  can be seen a concatenation between  $\tilde{\mathbf{G}}_{(i^+)}$  and  $\tilde{\mathbf{G}}_{(j^-)}$ . Thus, the objective in 11 can be expanded as follows:

$$\begin{aligned} & \min_{\tilde{\mathbf{A}}, \tilde{\mathbf{B}}} \sum_{\forall [i,j] \in S} d\left(\text{ConvexHull}\left(\mathcal{Z}_{\tilde{\mathbf{G}}_{(i^+, j^-)}}, \mathcal{Z}_{\tilde{\mathbf{G}}_{(j^+, i^-)}}\right), \text{ConvexHull}\left(\mathcal{Z}_{\mathbf{G}_{(i^+, j^-)}}, \mathcal{Z}_{\mathbf{G}_{(j^+, i^-)}}\right)\right) \\ &= \min_{\tilde{\mathbf{A}}, \tilde{\mathbf{B}}} \sum_{\forall [i,j] \in S} d\left(\text{ConvexHull}\left(\mathcal{Z}_{\tilde{\mathbf{G}}_{i^+}} \tilde{+} \mathcal{Z}_{\tilde{\mathbf{G}}_{j^-}}, \mathcal{Z}_{\tilde{\mathbf{G}}_{j^+}} \tilde{+} \mathcal{Z}_{\tilde{\mathbf{G}}_{i^-}}\right), \text{ConvexHull}\left(\mathcal{Z}_{\mathbf{G}_{i^+}} \tilde{+} \mathcal{Z}_{\mathbf{G}_{j^-}}, \mathcal{Z}_{\mathbf{G}_{j^+}} \tilde{+} \mathcal{Z}_{\mathbf{G}_{i^-}}\right)\right) \\ &\approx \min_{\tilde{\mathbf{A}}, \tilde{\mathbf{B}}} \sum_{\forall [i,j] \in S} \left\| \begin{pmatrix} \tilde{\mathbf{G}}_{i^+} \\ \mathbf{G}_{j^-} \end{pmatrix} - \begin{pmatrix} \tilde{\mathbf{G}}_{i^+} \\ \mathbf{G}_{j^-} \end{pmatrix} \right\|_F^2 + \left\| \begin{pmatrix} \tilde{\mathbf{G}}_{i^-} \\ \mathbf{G}_{j^+} \end{pmatrix} - \begin{pmatrix} \tilde{\mathbf{G}}_{i^-} \\ \mathbf{G}_{j^+} \end{pmatrix} \right\|_F^2 \\ &= \min_{\tilde{\mathbf{A}}, \tilde{\mathbf{B}}} \sum_{\forall [i,j] \in S} \frac{1}{2} \left\| \tilde{\mathbf{G}}_{i^+} - \mathbf{G}_{i^+} \right\|_F^2 + \frac{1}{2} \left\| \tilde{\mathbf{G}}_{i^-} - \mathbf{G}_{i^-} \right\|_F^2 + \frac{1}{2} \left\| \tilde{\mathbf{G}}_{j^+} - \mathbf{G}_{j^+} \right\|_F^2 + \frac{1}{2} \left\| \tilde{\mathbf{G}}_{j^-} - \mathbf{G}_{j^-} \right\|_F^2 \\ &= \min_{\tilde{\mathbf{A}}, \tilde{\mathbf{B}}} \sum_{i=1}^k \frac{1}{2} (k-1) \left( \left\| \tilde{\mathbf{G}}_{i^+} - \mathbf{G}_{i^+} \right\|_F^2 + \left\| \tilde{\mathbf{G}}_{i^-} - \mathbf{G}_{i^-} \right\|_F^2 + \left\| \tilde{\mathbf{G}}_{j^+} - \mathbf{G}_{j^+} \right\|_F^2 + \left\| \tilde{\mathbf{G}}_{j^-} - \mathbf{G}_{j^-} \right\|_F^2 \right). \end{aligned}$$

The approximation follows in a similar argument to the binary classifier case where approximating the generators. The last equality follows from a counting argument. We solve the objective for all multi-class networks in the experiments with alternating optimization in a similar fashion to the binary classifier case. Similarly to the binary classification approach, we introduce the  $\|\cdot\|_{2,1}$  to enforce sparsity constraints for pruning purposes. Therefore the overall objective has the form:

$$\begin{aligned} & \min_{\tilde{\mathbf{A}}, \tilde{\mathbf{B}}} \sum_{i=1}^k \frac{1}{2} \left( \left\| \tilde{\mathbf{G}}_{i^+} - \mathbf{G}_{i^+} \right\|_F^2 + \left\| \tilde{\mathbf{G}}_{i^-} - \mathbf{G}_{i^-} \right\|_F^2 + \left\| \tilde{\mathbf{G}}_{j^+} - \mathbf{G}_{j^+} \right\|_F^2 + \left\| \tilde{\mathbf{G}}_{j^-} - \mathbf{G}_{j^-} \right\|_F^2 \right) \\ & \quad + \lambda \left( \left\| \tilde{\mathbf{G}}_{i^+} \right\|_{2,1} + \left\| \tilde{\mathbf{G}}_{i^-} \right\|_{2,1} + \left\| \tilde{\mathbf{G}}_{j^+} \right\|_{2,1} + \left\| \tilde{\mathbf{G}}_{j^-} \right\|_{2,1} \right). \end{aligned}$$

For completion, we derive the updates for  $\tilde{\mathbf{A}}$  and  $\tilde{\mathbf{B}}$ .



**Update  $\tilde{\mathbf{A}}$ .**

$$\begin{aligned} \tilde{\mathbf{A}} = \arg \min_{\tilde{\mathbf{A}}} \sum_{i=1}^k \frac{1}{2} & \left( \left\| \text{Diag} \left( \tilde{\mathbf{B}}^+(i, :) \right) \tilde{\mathbf{A}} - \mathbf{G}_{i+} \right\|_F^2 + \left\| \text{Diag} \left( \tilde{\mathbf{B}}^-(i, :) \right) \tilde{\mathbf{A}} - \mathbf{G}_{i-} \right\|_F^2 \right. \\ & + \left\| \text{Diag} \left( \tilde{\mathbf{B}}^+(j, :) \right) \tilde{\mathbf{A}} - \mathbf{G}_{j+} \right\|_F^2 + \left\| \text{Diag} \left( \tilde{\mathbf{B}}^-(j, :) \right) \tilde{\mathbf{A}} - \mathbf{G}_{j-} \right\|_F^2 \Big) \\ & + \lambda \left( \left\| \text{Diag} \left( \tilde{\mathbf{B}}^+(i, :) \right) \tilde{\mathbf{A}} \right\|_{2,1} + \left\| \text{Diag} \left( \tilde{\mathbf{B}}^-(i, :) \right) \tilde{\mathbf{A}} \right\|_{2,1} + \left\| \text{Diag} \left( \tilde{\mathbf{B}}^+(j, :) \right) \tilde{\mathbf{A}} \right\|_{2,1} \right. \\ & \left. + \left\| \text{Diag} \left( \tilde{\mathbf{B}}^-(j, :) \right) \tilde{\mathbf{A}} \right\|_{2,1} \right). \end{aligned}$$

Similar to the binary classification, the problem is separable in the rows of  $\tilde{\mathbf{A}}$ . and a closed form solution in terms of the proximal operator of  $\ell_2$  norm follows naturally for each  $\tilde{\mathbf{A}}(i, :)$ .

**Update  $\tilde{\mathbf{B}}^+(i, :)$ .**

$$\tilde{\mathbf{B}}^+(i, :) = \arg \min_{\tilde{\mathbf{B}}^+(i, :)} \frac{1}{2} \left\| \text{Diag} \left( \tilde{\mathbf{B}}^+(i, :) \right) \tilde{\mathbf{A}} - \tilde{\mathbf{G}}_{i+} \right\|_F^2 + \lambda \left\| \text{Diag} \left( \tilde{\mathbf{B}}^+(i, :) \right) \tilde{\mathbf{A}} \right\|_{2,1}, \quad \text{s.t. } \tilde{\mathbf{B}}^+(i, :) \geq \mathbf{0}.$$

Note that the problem is separable per coordinates of  $\tilde{\mathbf{B}}^+(i, :)$  and each subproblem is updated as:

$$\begin{aligned} \tilde{\mathbf{B}}^+(i, j) &= \arg \min_{\tilde{\mathbf{B}}^+(i, j)} \frac{1}{2} \left\| \tilde{\mathbf{B}}^+(i, j) \tilde{\mathbf{A}}(j, :) - \tilde{\mathbf{G}}_{i+}(j, :) \right\|_2^2 + \lambda \left\| \tilde{\mathbf{B}}^+(i, j) \tilde{\mathbf{A}}(j, :) \right\|_2, \quad \text{s.t. } \tilde{\mathbf{B}}^+(i, j) \geq 0 \\ &= \arg \min_{\tilde{\mathbf{B}}^+(i, j)} \frac{1}{2} \left\| \tilde{\mathbf{B}}^+(i, j) \tilde{\mathbf{A}}(j, :) - \tilde{\mathbf{G}}_{i+}(j, :) \right\|_2^2 + \lambda \left| \tilde{\mathbf{B}}^+(i, j) \right| \left\| \tilde{\mathbf{A}}(j, :) \right\|_2, \quad \text{s.t. } \tilde{\mathbf{B}}^+(i, j) \geq 0 \\ &= \max \left( 0, \frac{\tilde{\mathbf{A}}(j, :)^\top \tilde{\mathbf{G}}_{i+}(j, :) - \lambda \left\| \tilde{\mathbf{A}}(j, :) \right\|_2}{\left\| \tilde{\mathbf{A}}(j, :) \right\|_2^2} \right). \end{aligned}$$

A similar argument can be used to update  $\tilde{\mathbf{B}}^-(i, :)$   $\forall i$ . Finally, the parameters of the pruned network will be constructed  $\mathbf{A} \leftarrow \tilde{\mathbf{A}}$  and  $\mathbf{B} \leftarrow \tilde{\mathbf{B}}^+ - \tilde{\mathbf{B}}^-$ .

**Algorithm 1** Solving Problem (5)

**Input:**  $\mathbf{A}_1 \in \mathbb{R}^{p \times n}$ ,  $\mathbf{B} \in \mathbb{R}^{k \times p}$ ,  $\mathbf{x}_0 \in \mathbb{R}^n$ ,  $t, \lambda > 0, \gamma > 1, K > 0, \xi_{\mathbf{A}_1} = \mathbf{0}_{p \times n}, \eta^1 = \mathbf{z}^1 = \mathbf{w}^1 = \mathbf{z}^1 = \mathbf{u}^1 = \mathbf{w}^1 = \mathbf{0}_n$ .

**Output:**  $\eta, \xi_{\mathbf{A}_1}$ 
**Initialize:**  $\rho = \rho_0$ 
**while** not converged **do**

   **for**  $k \leq K$  **do**

      **$\eta$  update:**  $\eta^{k+1} = (2\lambda \mathbf{A}_1^\top \mathbf{A}_1 + (2 + \rho)\mathbf{I})^{-1}(2\lambda \mathbf{A}_1^\top \xi_{\mathbf{A}_1}^k \mathbf{x}_0 + \rho \mathbf{z}^k - \mathbf{u}^k)$ 

      **$\mathbf{w}$  update:**  $\mathbf{w}^{k+1} = \begin{cases} \min(1 - \mathbf{x}_0, \epsilon_1) & : \mathbf{z}^k - 1/\rho \mathbf{v}^k > \min(1 - \mathbf{x}_0, \epsilon_1) \\ \max(-\mathbf{x}_0, -\epsilon_1) & : \mathbf{z}^k - 1/\rho \mathbf{v}^k < \max(-\mathbf{x}_0, -\epsilon_1) \\ \mathbf{z}^k - 1/\rho \mathbf{v}^k & : \text{otherwise} \end{cases}$ 

      **$\mathbf{z}$  update:**  $\mathbf{z}^{k+1} = \frac{1}{\eta^{k+1} + 2\rho}(\eta^{k+1} \mathbf{z}^k + \rho(\eta^{k+1} + 1/\rho \mathbf{u}^k + \mathbf{w}^k + 1/\rho \mathbf{v}^k) - \nabla \mathcal{L}(\mathbf{z}^k + \mathbf{x}_0))$ 

      **$\xi_{\mathbf{A}_1}$  update:**  $\xi_{\mathbf{A}_1}^{k+1} = \arg \min_{\xi_{\mathbf{A}_1}} \|\xi_{\mathbf{A}_1}\|_F^2 + \lambda \|\xi_{\mathbf{A}_1} \mathbf{x}_0 - \mathbf{A}_1 \eta^{k+1}\|_2^2 + \tilde{\mathcal{L}}(\mathbf{A}_1)$  s.t.  $\|\xi_{\mathbf{A}_1}\|_{\infty, \infty} \leq \epsilon_2$ 

      **$\mathbf{u}$  update:**  $\mathbf{u}^{k+1} = \mathbf{u}^k + \rho(\eta^{k+1} - \mathbf{z}^{k+1})$ 

      **$\mathbf{v}$  update:**  $\mathbf{v}^{k+1} = \mathbf{v}^k + \rho(\mathbf{w}^{k+1} - \mathbf{z}^{k+1})$ 

      $\rho \leftarrow \gamma \rho$ 

   **end**

    $\lambda \leftarrow \gamma \lambda$ 

    $\rho \leftarrow \rho_0$ 
**end**
**E. Algorithm for Solving 5.**

In this section, we are going to derive an algorithm for solving the following problem:

$$\begin{aligned}
 \min_{\eta, \xi_{\mathbf{A}_1}} \quad & \mathcal{D}_1(\eta) + \mathcal{D}_2(\xi_{\mathbf{A}_1}) \\
 \text{s.t.} \quad & -\text{loss}(g(\mathbf{A}_1(\mathbf{x}_0 + \eta)), t) \leq -1, \quad -\text{loss}(g(\mathbf{A}_1 + \xi_{\mathbf{A}_1})\mathbf{x}_0, t) \leq -1, \\
 & (\mathbf{x}_0 + \eta) \in [0, 1]^n, \quad \|\eta\|_\infty \leq \epsilon_1, \quad \|\xi_{\mathbf{A}_1}\|_{\infty, \infty} \leq \epsilon_2, \quad \mathbf{A}_1 \eta - \xi_{\mathbf{A}_1} \mathbf{x}_0 = 0.
 \end{aligned} \tag{12}$$

The function  $\mathcal{D}_2(\xi_{\mathbf{A}_1})$  captures the perturbation in the dual subdivision polytope such that the dual subdivision of the network with the first linear layer  $\mathbf{A}_1$  is similar to the dual subdivision of the network with the first linear layer  $\mathbf{A}_1 + \xi_{\mathbf{A}_1}$ . This can be generally formulated as an approximation to the following distance function  $d(\text{ConvHull}(\mathcal{Z}_{\tilde{\mathbf{G}}_1}, \mathcal{Z}_{\tilde{\mathbf{G}}_2}), \text{ConvHull}(\mathcal{Z}_{\mathbf{G}_1}, \mathcal{Z}_{\mathbf{G}_2}))$ , where  $\tilde{\mathbf{G}}_1 = \text{Diag}[\text{ReLU}(\tilde{\mathbf{B}}(1, :)) + \text{ReLU}(-\tilde{\mathbf{B}}(2, :))] (\tilde{\mathbf{A}} + \xi_{\mathbf{A}_1})$ ,  $\tilde{\mathbf{G}}_2 = \text{Diag}[\text{ReLU}(\tilde{\mathbf{B}}(2, :)) + \text{ReLU}(-\tilde{\mathbf{B}}(1, :))] (\tilde{\mathbf{A}} + \xi_{\mathbf{A}_1})$ ,  $\mathbf{G}_1 = \text{Diag}[\text{ReLU}(\tilde{\mathbf{B}}(1, :)) + \text{ReLU}(-\tilde{\mathbf{B}}(2, :))] \tilde{\mathbf{A}}$  and  $\mathbf{G}_2 = \text{Diag}[\text{ReLU}(\tilde{\mathbf{B}}(2, :)) + \text{ReLU}(-\tilde{\mathbf{B}}(1, :))] \tilde{\mathbf{A}}$ . In particular, to approximate the function  $d$ , one can use a similar argument as in used in network pruning 5 such that  $\mathcal{D}_2$  approximates the generators of the zonotopes directly as follows:

$$\begin{aligned}
 \mathcal{D}_2(\xi_{\mathbf{A}_1}) &= \frac{1}{2} \|\tilde{\mathbf{G}}_1 - \mathbf{G}_1\|_F^2 + \frac{1}{2} \|\tilde{\mathbf{G}}_2 - \mathbf{G}_2\|_F^2 \\
 &= \frac{1}{2} \|\text{Diag}(\mathbf{B}^+(1, :)) \xi_{\mathbf{A}_1}\|_F^2 + \frac{1}{2} \|\text{Diag}(\mathbf{B}^-(1, :)) \xi_{\mathbf{A}_1}\|_F^2 \\
 &\quad + \frac{1}{2} \|\text{Diag}(\mathbf{B}^+(2, :)) \xi_{\mathbf{A}_1}\|_F^2 + \frac{1}{2} \|\text{Diag}(\mathbf{B}^-(2, :)) \xi_{\mathbf{A}_1}\|_F^2.
 \end{aligned}$$

This can thereafter be extended to multi-class network with  $k$  classes as follows  $\mathcal{D}_2(\xi_{\mathbf{A}_1}) = \frac{1}{2} \sum_{j=1}^k \|\text{Diag}(\mathbf{B}^+(j, :)) \xi_{\mathbf{A}_1}\|_F^2 + \|\text{Diag}(\mathbf{B}^-(j, :)) \xi_{\mathbf{A}_1}\|_F^2$ . Following (Xu et al., 2018), we take  $\mathcal{D}_1(\eta) = \frac{1}{2} \|\eta\|_2^2$ . Therefore, we can write 12 as follows:

$$\begin{aligned}
 \min_{\eta, \xi_{\mathbf{A}}} \quad & \mathcal{D}_1(\eta) + \sum_{j=1}^k \left\| \text{Diag}(\mathbf{B}^+(j, :)) \xi_{\mathbf{A}} \right\|_F^2 + \left\| \text{Diag}(\mathbf{B}^-(j, :)) \xi_{\mathbf{A}} \right\|_F^2. \\
 \text{s.t.} \quad & -\text{loss}(g(\mathbf{A}_1(\mathbf{x}_0 + \eta)), t) \leq -1, \quad -\text{loss}(g((\mathbf{A}_1 + \xi_{\mathbf{A}_1})\mathbf{x}_0), t) \leq -1, \\
 & (\mathbf{x}_0 + \eta) \in [0, 1]^n, \quad \|\eta\|_\infty \leq \epsilon_1, \quad \|\xi_{\mathbf{A}_1}\|_{\infty, \infty} \leq \epsilon_2, \quad \mathbf{A}_1\eta - \xi_{\mathbf{A}_1}\mathbf{x}_0 = 0.
 \end{aligned}$$

To enforce the linear equality constraints  $\mathbf{A}_1\eta - \xi_{\mathbf{A}_1}\mathbf{x}_0 = 0$ , we use a penalty method, where each iteration of the penalty method we solve the sub-problem with ADMM updates. That is, we solve the following optimization problem with ADMM with increasing  $\lambda$  such that  $\lambda \rightarrow \infty$ . For ease of notation, let's denote  $\mathcal{L}(\mathbf{x}_0 + \eta) = -\text{loss}(g(\mathbf{A}_1(\mathbf{x}_0 + \eta)), t)$ , and  $\bar{\mathcal{L}}(\mathbf{A}_1) = -\text{loss}(g((\mathbf{A}_1 + \xi_{\mathbf{A}_1})\mathbf{x}_0), t)$ .

$$\begin{aligned}
 \min_{\eta, \mathbf{z}, \mathbf{w}, \xi_{\mathbf{A}_1}} \quad & \|\eta\|_2^2 + \sum_{j=1}^k \left\| \text{Diag}(\text{ReLU}(\mathbf{B}(j, :))) \xi_{\mathbf{A}_1} \right\|_F^2 + \left\| \text{Diag}(\text{ReLU}(-\mathbf{B}(j, :))) \xi_{\mathbf{A}_1} \right\|_F^2 \\
 & + \mathcal{L}(\mathbf{x}_0 + \mathbf{z}) + h_1(\mathbf{w}) + h_2(\xi_{\mathbf{A}_1}) + \lambda \|\mathbf{A}_1\eta - \xi_{\mathbf{A}_1}\mathbf{x}_0\|_2^2 + \bar{\mathcal{L}}(\mathbf{A}_1). \\
 \text{s.t.} \quad & \eta = \mathbf{z} \quad \mathbf{z} = \mathbf{w}.
 \end{aligned}$$

where

$$h_1(\eta) = \begin{cases} 0, & \text{if } (\mathbf{x}_0 + \eta) \in [0, 1]^n, \|\eta\|_\infty \leq \epsilon_1 \\ \infty, & \text{else} \end{cases} \quad h_2(\xi_{\mathbf{A}_1}) = \begin{cases} 0, & \text{if } \|\xi_{\mathbf{A}_1}\|_{\infty, \infty} \leq \epsilon_2 \\ \infty, & \text{else} \end{cases}.$$

The augmented Lagrangian is given as follows:

$$\begin{aligned}
 \mathcal{L}(\eta, \mathbf{w}, \mathbf{z}, \xi_{\mathbf{A}_1}, \mathbf{u}, \mathbf{v}) := \quad & \|\eta\|_2^2 + \mathcal{L}(\mathbf{x}_0 + \mathbf{z}) + h_1(\mathbf{w}) + \sum_{j=1}^k \left\| \text{Diag}(\mathbf{B}^+(j, :)) \xi_{\mathbf{A}_1} \right\|_F^2 + \left\| \text{Diag}(\mathbf{B}^-(j, :)) \xi_{\mathbf{A}_1} \right\|_F^2 \\
 & + \bar{\mathcal{L}}(\mathbf{A}_1) + h_2(\xi_{\mathbf{A}_1}) + \lambda \|\mathbf{A}_1\eta - \xi_{\mathbf{A}_1}\mathbf{x}_0\|_2^2 + \mathbf{u}^\top (\eta - \mathbf{z}) + \mathbf{v}^\top (\mathbf{w} - \mathbf{z}) \\
 & + \frac{\rho}{2} (\|\eta - \mathbf{z}\|_2^2 + \|\mathbf{w} - \mathbf{z}\|_2^2).
 \end{aligned}$$

Thereafter, ADMM updates are given as follows:

$$\begin{aligned}
 \{\eta^{k+1}, \mathbf{w}^{k+1}\} &= \arg \min_{\eta, \mathbf{w}} \mathcal{L}(\eta, \mathbf{w}, \mathbf{z}^k, \xi_{\mathbf{A}_1}^k, \mathbf{u}^k, \mathbf{v}^k), \\
 \mathbf{z}^{k+1} &= \arg \min_{\mathbf{z}} \mathcal{L}(\eta^{k+1}, \mathbf{w}^{k+1}, \mathbf{z}, \xi_{\mathbf{A}_1}^k, \mathbf{u}^k, \mathbf{v}^k), \\
 \xi_{\mathbf{A}_1}^{k+1} &= \arg \min_{\xi_{\mathbf{A}_1}} \mathcal{L}(\eta^{k+1}, \mathbf{w}^{k+1}, \mathbf{z}^{k+1}, \xi_{\mathbf{A}_1}, \mathbf{u}^k, \mathbf{v}^k). \\
 \mathbf{u}^{k+1} &= \mathbf{u}^k + \rho(\eta^{k+1} - \mathbf{z}^{k+1}), \quad \mathbf{v}^{k+1} = \mathbf{v}^k + \rho(\mathbf{w}^{k+1} - \mathbf{z}^{k+1}).
 \end{aligned}$$

**Updating  $\eta$ :**

$$\begin{aligned}
 \eta^{k+1} &= \arg \min_{\eta} \|\eta\|_2^2 + \lambda \|\mathbf{A}_1\eta - \xi_{\mathbf{A}_1}\mathbf{x}_0\|_2^2 + \mathbf{u}^\top \eta + \frac{\rho}{2} \|\eta - \mathbf{z}\|_2^2 \\
 &= \left( 2\lambda \mathbf{A}_1^\top \mathbf{A}_1 + (2 + \rho) \mathbf{I} \right)^{-1} \left( 2\lambda \mathbf{A}_1^\top \xi_{\mathbf{A}_1}^k \mathbf{x}_0 + \rho \mathbf{z}^k - \mathbf{u}^k \right).
 \end{aligned}$$

**Updating  $\mathbf{w}$ :**

$$\begin{aligned}\mathbf{w}^{k+1} &= \arg \min_{\mathbf{w}} \mathbf{v}^{k\top} \mathbf{w} + h_1(\mathbf{w}) + \frac{\rho}{2} \|\mathbf{w} - \mathbf{z}^k\|_2^2 \\ &= \arg \min_{\mathbf{w}} \frac{1}{2} \left\| \mathbf{w} - \left( \mathbf{z}^k - \frac{\mathbf{v}^k}{\rho} \right) \right\|_2^2 + \frac{1}{\rho} h_1(\mathbf{w}).\end{aligned}$$

The update  $\mathbf{w}$  is separable in coordinates as follows:

$$\mathbf{w}^{k+1} = \begin{cases} \min(1 - \mathbf{x}_0, \epsilon_1) & : \mathbf{z}^k - 1/\rho \mathbf{v}^k > \min(1 - \mathbf{x}_0, \epsilon_1) \\ \max(-\mathbf{x}_0, -\epsilon_1) & : \mathbf{z}^k - 1/\rho \mathbf{v}^k < \max(-\mathbf{x}_0, -\epsilon_1) \\ \mathbf{z}^k - 1/\rho \mathbf{v}^k & : \textit{otherwise} \end{cases}$$

**Updating  $\mathbf{z}$ :**

$$\mathbf{z}^{k+1} = \arg \min_{\mathbf{z}} \mathcal{L}(\mathbf{x}_0 + \mathbf{z}) - \mathbf{u}^{k\top} \mathbf{z} - \mathbf{v}^{k\top} \mathbf{z} + \frac{\rho}{2} (\|\eta^{k+1} - \mathbf{z}\|_2^2 + \|\mathbf{w}^{k+1} - \mathbf{z}\|_2^2).$$

(Liu et al., 2019) showed that the linearized ADMM converges for some non-convex problems. Therefore, by linearizing  $\mathcal{L}$  and adding Bergman divergence term  $\eta^k/2 \|\mathbf{z} - \mathbf{z}^k\|_2^2$ , we can then update  $\mathbf{z}$  as follows:

$$\mathbf{z}^{k+1} = \frac{1}{\eta^k + 2\rho} \left( \eta^k \mathbf{z}^k + \rho(\eta^{k+1} + \frac{1}{\rho} \mathbf{u}^k + \mathbf{w}^{k+1} + \frac{1}{\rho} \mathbf{v}^k) - \nabla \mathcal{L}(\mathbf{z}^k + \mathbf{x}_0) \right).$$

It is worthy to mention that the analysis until this step is inspired by (Xu et al., 2018) with modifications to adapt our new formulation.

**Updating  $\xi_{\mathbf{A}}$ :**

$$\xi_{\mathbf{A}}^{k+1} = \arg \min_{\xi_{\mathbf{A}}} \|\xi_{\mathbf{A}_1}\|_F^2 + \lambda \|\xi_{\mathbf{A}_1} \mathbf{x}_0 - \mathbf{A}_1 \eta\|_2^2 + \bar{\mathcal{L}}(\mathbf{A}_1) \text{ s.t. } \|\xi_{\mathbf{A}_1}\|_{\infty, \infty} \leq \epsilon_2.$$

The previous problem can be solved with proximal gradient methods.



## F. Experimental Details and Supplemental Results

In this section, we describe the settings and the values of the hyper parameters used in the experiments. Moreover, we will show some further supplemental results to the results in the main manuscript paper.

### F.1. Tropical View to the Lottery Ticket Hypothesis.

We first conduct some further supplemental experiments to those conducted in Section 4. In particular, we conduct further experiments re-affirming the lottery ticket hypothesis on three more synthetic datasets in a similar experimental setup to the one shown in Figure 3. The new supplemental experiments are shown in Figure 7. A similar conclusion is present where the lottery ticket initialization consistently better preserves the decision boundaries polytope compare to other initialization schemes over different percentages of pruning.

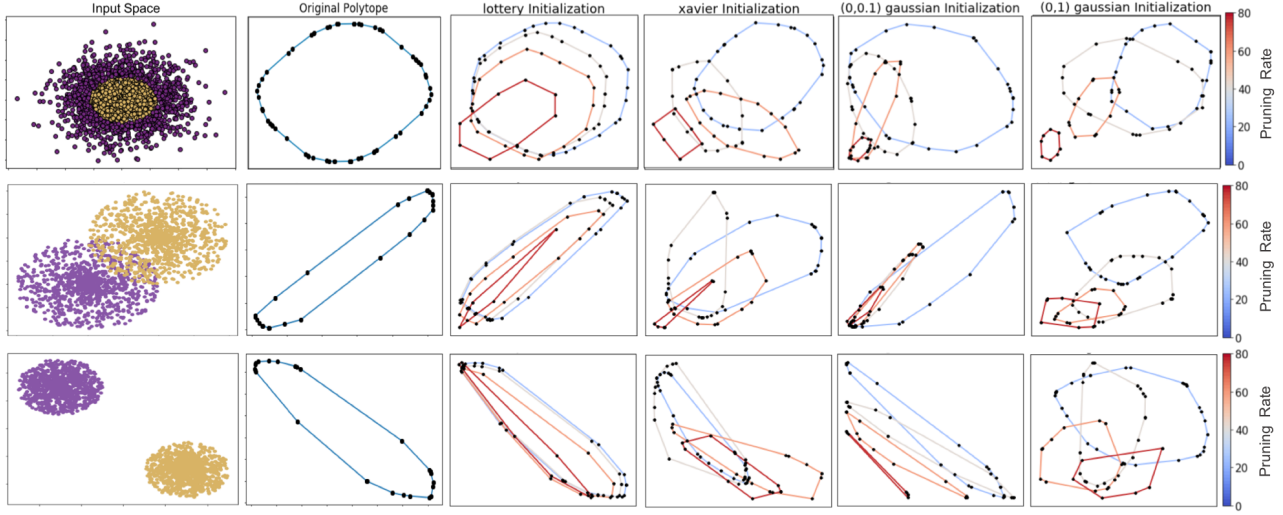
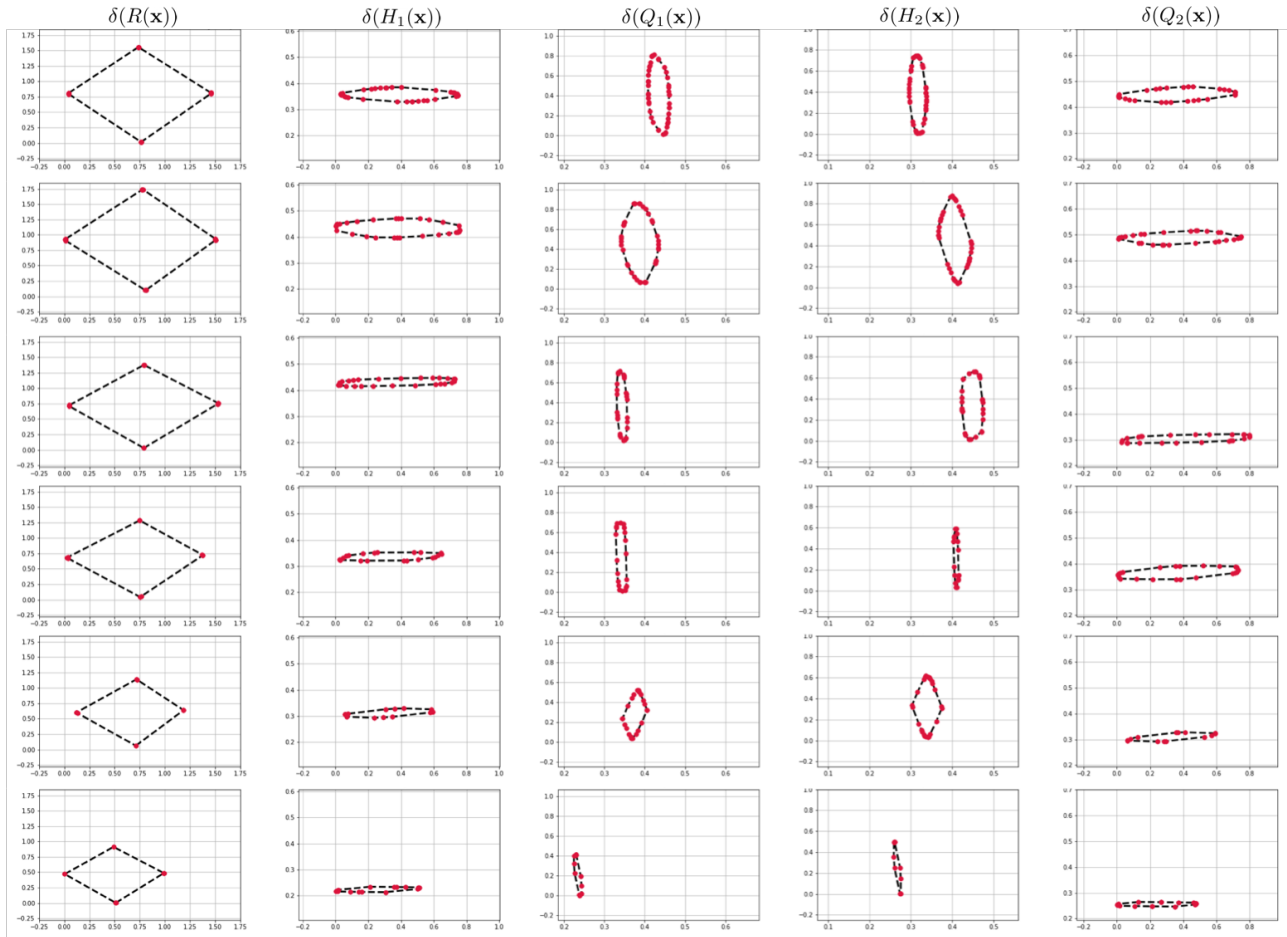


Figure 7. **Effect of Different Initializations on the Decision Boundaries Polytope.** From left to right: training dataset, decision boundaries polytope of original network followed by the decision boundaries polytope during several iterations of pruning with different initializations.

A natural question is whether it is necessary to visualize the dual subdivision polytope of the decision boundaries, *i.e.*  $\delta(R(\mathbf{x}))$ , where  $R(\mathbf{x}) = H_1(\mathbf{x}) \odot Q_2(\mathbf{x}) \oplus H_2(\mathbf{x}) \odot Q_1(\mathbf{x})$  as opposed to visualizing the tropical polynomials  $\delta(H_{\{1,2\}}(\mathbf{x}))$  and  $\delta(Q_{\{1,2\}}(\mathbf{x}))$  directly for the tropical re-affirmation of the lottery ticket hypothesis. That is similar to asking whether it is necessary to visualize and study the decision boundaries polytope  $\delta(R(\mathbf{x}))$  as compared to the the dual subdivision polytope of the functional form of the network since for the 2-output neural network described in Theorem 2 we have that  $f_1(\mathbf{x}) = H_1(\mathbf{x}) \odot Q_1(\mathbf{x})$  and  $f_2(\mathbf{x}) = H_2(\mathbf{x}) \odot Q_2(\mathbf{x})$ . We demonstrate this with an experiment that demonstrates the differences between these two views. For this purpose, we train a single hidden layer neural network on the same dataset shown in Figure 3. We perform several iterations of pruning in a similar fashion to Section 5 and visualise at each iteration both the decision boundaries polytope and all the dual subdivisions of the aforementioned tropical polynomials representing the functional form of the network, *i.e.*  $\delta(H_{\{1,2\}}(\mathbf{x}))$  and  $\delta(Q_{\{1,2\}}(\mathbf{x}))$ . It is to be observed from Figure 8 that despite that the decision boundaries were barely affected with the lottery ticket pruning, the zonotopes representing the functional form of the network endure large variations. That is to say, investigating the dual subdivisions describing the functional form of the networks through the four zonotopes  $\delta(H_{\{1,2\}}(\mathbf{x}))$  and  $\delta(Q_{\{1,2\}}(\mathbf{x}))$  is not indicative enough to the behaviour of the decision boundaries.



**Figure 8. Comparison between the decision boundaries polytope and the polytopes representing the functional representation of the network.** First column: decision boundaries polytope  $\delta(R(\mathbf{x}))$  while the remainder of the columns are the zonotopes  $\delta(H_1(\mathbf{x}))$ ,  $\delta(Q_1(\mathbf{x}))$ ,  $\delta(H_2(\mathbf{x}))$  and  $\delta(Q_2(\mathbf{x}))$  respectively. Under varying pruning rate across the rows, it is to be observed that the changes that affected the dual subdivisions of the functional representations are far smaller compared to the decision boundaries polytope.

## F.2. Tropical Pruning

**Experimental Setup.** In all experiments of the tropical pruning section, all algorithms are run for only a single iteration where  $\lambda$  increases linearly from 0.02 with a factor of 0.01. Increasing  $\lambda$  corresponds to increasing weight sparsity and we keep doing until sparsification is 100%.

**Supplemental Experiments.** We conduct more experimental results on AlexNet and VGG16 on SVHN, CIFAR10 and CIFAR100 datasets. We examine the performance for when the networks have only the biases of the classifier fine tuned after tuning as shown in Figure 9. Moreover, a similar experiments is reported for the same networks but for when the biases for the complete networks are fine tuned as in Figure 10.

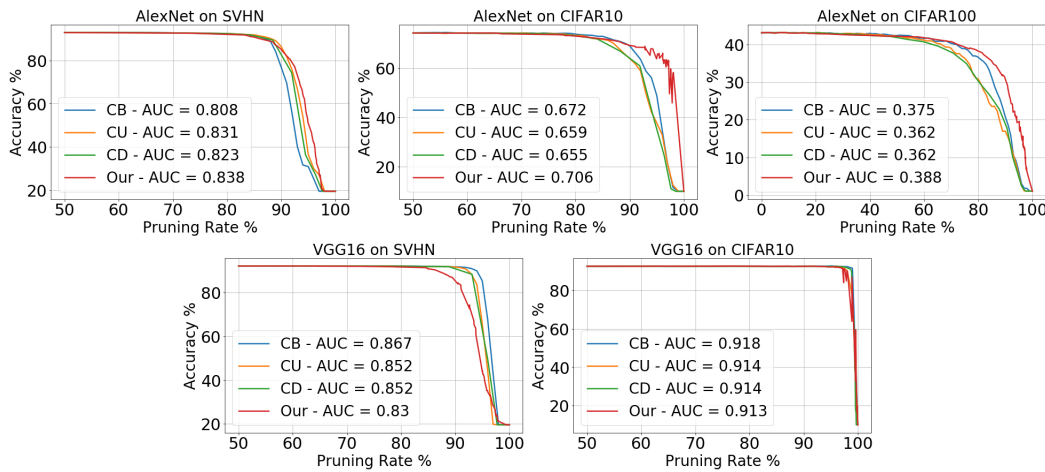


Figure 9. Results of Tropical Pruning with Fine Tuning the Biases of the Classifier. Tropical pruning applied on AlexNet and VGG16 trained on SVHN, CIFAR10, CIFAR100 against different pruning methods with fine tuning the biases of the classifier only.

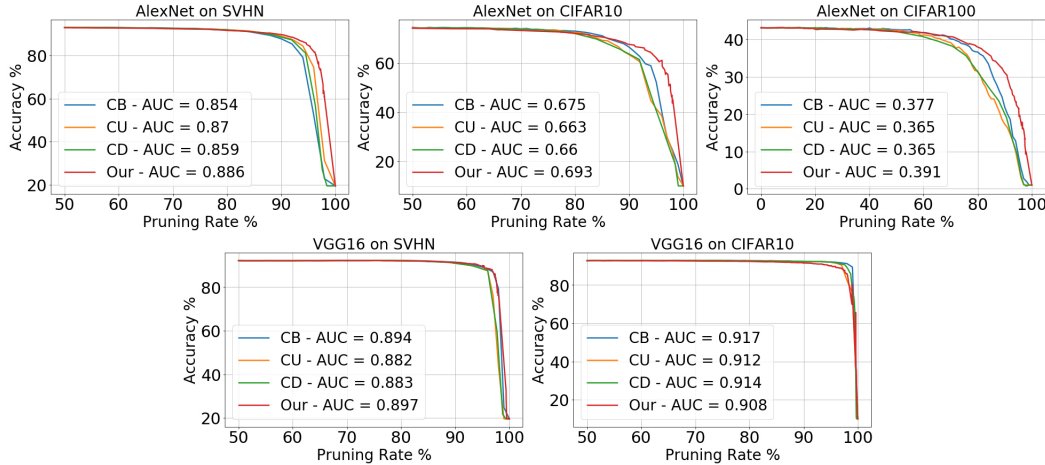


Figure 10. Results of Tropical Pruning with Fine Tuning the Biases of the Network. Tropical pruning applied on AlexNet and VGG16 trained on SVHN, CIFAR10, CIFAR100 against different pruning methods with fine tuning the biases of the network.

### E.3. Tropical Adversarial Attacks

**Experimental Setup.** For the tropical adversarial attacks experiments, there are five different hyper parameters which are

- $\epsilon_1$  : The upper bound for the infinite norm of  $\delta$ .
- $\epsilon_2$  : The upper bound for the  $\|\cdot\|_{\infty, \infty}$  of the perturbation on the first linear layer.
- $\lambda$  : Regularizer to enforce the equality between input perturbation and first layer perturbation
- $\eta$  : Bergman divergence constant.
- $\rho$  : ADMM constant.

For all of the experiments, we set the values of  $\epsilon_2, \lambda, \eta$  and  $\rho$  to 1,  $10^{-3}$ , 2.5 and 1, respectively. As for  $\epsilon_1$  it is set to 0.1 upon attacking MNIST images of digit 4 set to 0.2 for all other MNIST images.

**Supplemental Synthetic Experiments.** We show extra results of attacking the decision boundaries of synthetic data in  $\mathbb{R}^2$  in a similar setting as reported in Section 6. Figure 11 shows another example where the sampled to be attacked is closer to a different decision boundary. Observe how the edge corresponding to that decision boundary of the decision boundary polytope has respectively been altered.

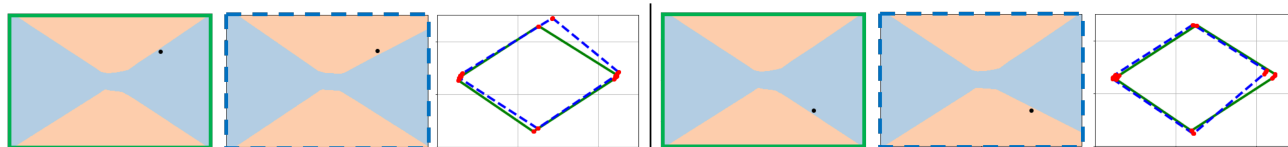


Figure 11. **Dual View of Tropical Adversarial Attacks.** Effect of tropical adversarial attack on a synthetic dataset with two classes in two different scenarios for the black input point. From left to right: decision boundaries of Original model, perturbed model and decision boundaries polytopes (green for original model and blue for perturbed model).

**MNIST Experiments.** Here, we design perturbations to misclassify MNIST images. Figure 12 shows several adversarial examples that change the network prediction for digits 8 and 9 to digits 7, 5, and 4, respectively. In some cases, the perturbation  $\eta$  is as small as  $\epsilon = 0.1$ , where  $\mathbf{x}_0 \in [0, 1]^n$ . Several other adversarial results are reported in Figure 13. We again emphasize that our approach is not meant to be compared with (or beat) state of the art adversarial attacks but rather to provide a novel geometrically inspired perspective that can shed new light in this field.

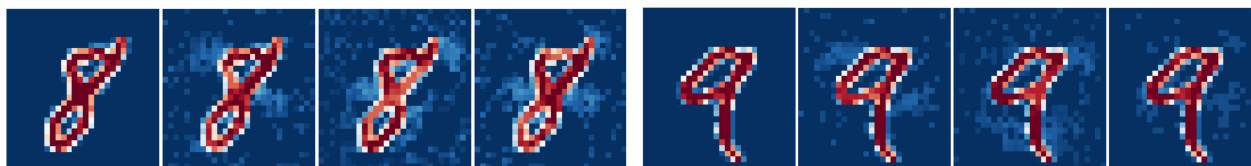
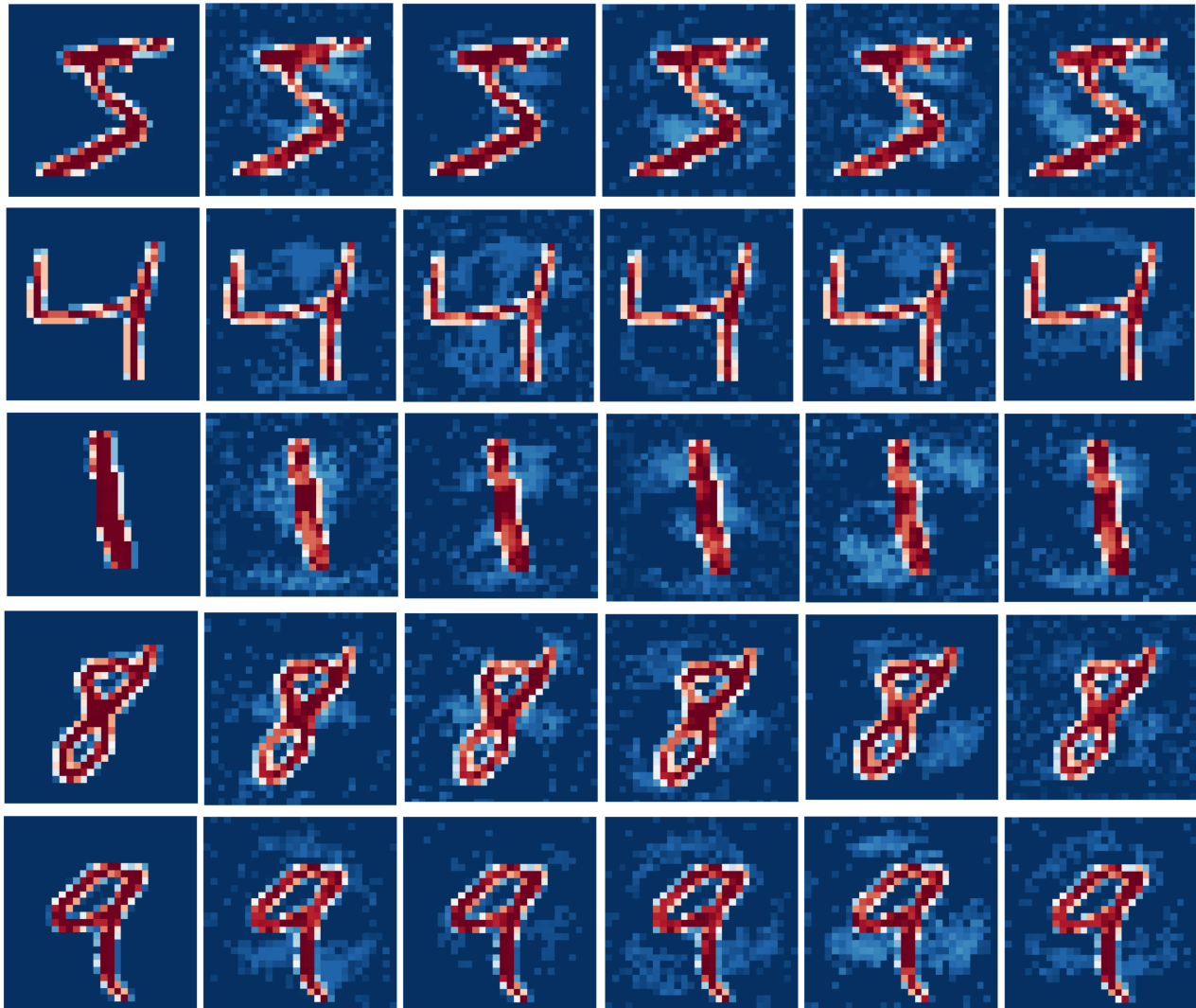


Figure 12. **Effect of Tropical Adversarial Attacks on MNIST Dataset.** We show qualitative examples of adversarial attacks, produced by solving Problem (5), on two digits (8,9) from MNIST. From left to right, images are classified as [8,7,5,4] and [9,7,5,4] respectively.





*Figure 13. Effect of Tropical Adversarial Attacks on MNIST Images.* First row from the left: Clean image, perturbed images classified as [7,3,2,1,0] respectively. Second row from left: Clean image, perturbed images classified as [9,8,7,3,2] respectively. Third row from left: Clean image, perturbed images classified as [9,8,7,5,3] respectively. Fourth row from left: Clean image, perturbed images classified as [9,4,3,2,1] respectively. Fifth row from left: Clean image, perturbed images classified as [8,4,3,2,1] respectively.